PSR Report 2248

PERFORMANCE REQUIREMENTS FOR LONG-STANDOFF-RANGE INFRARED IMAGING SENSOR

P. M. Moser

February 1992

Phase Report
Contract N62269-90-C-0551

Sponsored by
Naval Air Warfare Center
Aircraft Division Warminster
Warminster, PA 18974

PACIFIC-SIERRA RESEARCH CORPORATION
600 Louis Drive, Suite 103 • Warminster, Pennsylvania 18974 • (215) 441-4461
12340 Santa Monica Boulevard • Los Angeles, California 90025 • (213) 820-2200

REPORT DOCUMENTATION PAGE

Form Approved
OMB No. 0704-0188

1. REPORT DATE *(DD-MM-YYYY)*	2. REPORT TYPE	3. DATES COVERED *(From - To)*
xx-02-1992	Phase technical	To February 1992

4. TITLE AND SUBTITLE
Performance Requirements for Long-Standoff-Range Infrared Imaging Sensor

5a. CONTRACT NUMBER
Contract N62269-90-C-0551

5b. GRANT NUMBER

5c. PROGRAM ELEMENT NUMBER

6. AUTHOR(S)
Moser, Paul M.

5d. PROJECT NUMBER

5e. TASK NUMBER

5f. WORK UNIT NUMBER

7. PERFORMING ORGANIZATION NAME(S) AND ADDRESS(ES)
Pacific-Sierra Research Corporation
Warminster, PA 18974

8. PERFORMING ORGANIZATION REPORT NUMBER
PSR Report 2248

9. SPONSORING/MONITORING AGENCY NAME(S) AND ADDRESS(ES)
Naval Air Warfare Center Aircraft Division Warminster

10. SPONSOR/MONITOR'S ACRONYM(S)
NAWCADWAR

11. SPONSOR/MONITOR'S REPORT NUMBER(S)

12. DISTRIBUTION/AVAILABILITY STATEMENT
Approved for public release, distribution unlimited

13. SUPPLEMENTARY NOTES
See also PSR Report 2273, Performance Predictions for a Long-Standoff-Range Infrared Imaging Sensor" by the same author.

14. ABSTRACT
In the future, the contest for information will dominate maritime warfare, global surveillance will be routine, and battle spaces will expand. Accordingly, the U.S. Navy has a requirement for generating near-real-time, near-photographic-quality aerial imagery of a variety of targets from long standoff ranges both day and night. Missions include antisurface warfare, overland strike warfare, and intelligence. Targets range from large fixed installations such as power plants and bridges to relocatable anti-aircraft missile launchers and highly mobile vehicles. This report addresses the feasibility of developing a long-range infrared imaging sensor for satisfying such requirements.

15. SUBJECT TERMS
Long range, Infrared, Imaging, Sensor, Aircraft, Antisurface Warfare, Overland Strike Warfare, Intelligence

16. SECURITY CLASSIFICATION OF:			17. LIMITATION OF ABSTRACT	18. NUMBER OF PAGES	19a. NAME OF RESPONSIBLE PERSON
a. REPORT	b. ABSTRACT	c. THIS PAGE			19b. TELEPHONE NUMBER *(Include area code)*
unclassified	unclassified	unclassified	unlimited	57	

CONTENTS

INTRODUCTION

In its Navy-21 study, the National Research Council, Naval Studies Board[1] provided a "vision" of the Navy in the next 30 to 50 years which included the following:

> ► The contest for information will dominate maritime warfare. If the U.S. can achieve a significant advantage in both information gathering and interpretation, and in the denial of information to adversaries, this advantage will be decisive for success in maritime warfare.
>
> ► Global surveillance will be routine. Surveillance data will be integrated into a ubiquitous combat information network.
>
> ► Battle spaces will expand. Forces will cover more area while becoming more tightly integrated through the information system.

In line with the foregoing, the U.S. Navy has a requirement for generating near-real-time, near-photographic-quality aerial imagery of a variety of targets from long standoff ranges both day and night. The warfare areas that such a capability would support are Antisurface Warfare/War at Sea (ASUW/WAS), Overland Strike Warfare (STW), and Intelligence.

The applicable ASUW/WAS missions are to detect, identify, localize and track surface ships and boats. The STW mission includes surveillance and reconnaissance of land targets ranging from large fixed installations, such as power plants and bridges, to relocatable anti-aircraft missile launchers and highly mobile vehicles such as tanks and trucks. Intelligence includes gaining information necessary for Indication and Warning (I&W) and Threat Evaluation (TE). I&W includes observation of changes in a potential enemy's normal routines that might suggest an imminent attack. TE supports selection of an appropriate response based upon positions, velocities, classification, identification and number of targets and post-strike battle damage assessment. I&W and TE are distinguished by the completeness and quality (accuracy, update rate, resolution, sensitivity, etc.) of information about the threat.

The events of the past few years illustrate the difficulty of predicting where and when military conflicts will occur. (A basic premise of a major Navy study (Quo Vadis II) performed in 1988-89 was that the cold war would continue for the next 50

years.) The immortal words of Yogi Berra apply: "The future ain't what it used to be." It appears now that the world is heading into a new steady state of third world problems. It is likely that nuclear weapons and nuclear technology will spread to the less developed countries. The United Nations will become increasingly involved in "civil wars." It is expected that third world conflicts will be characterized by smaller, more mobile targets and short reaction times, non-western rules of engagement and nonconventional definitions of "victory." Actions that would appear completely irrational to western minds (such as setting oil wells on fire and dumping oil into the Persian Gulf) may become commonplace. More than ever before, it will be necessary to have flexible weapon systems that can be adapted to match the enemy and his environment. As the world becomes even more unglued, there will be an increasingly greater need for high quality information gathering systems.

It is expected that, for the foreseeable future, the Navy and Marine Corps will be concerned mostly with those regions that lie within ±150 nmi of the world's shorelines, i.e., near-land and limited over-land areas. There will be concern about weapons directed against a carrier battle group from small boats and from mobile and relocatable on-land missile launchers. In pre-hostility reconnaissance, the tactical aircraft serving as the platform for a long-standoff-range infrared imaging sensor might fly over international waters parallel to the coast line, acquiring imagery of boats being loaded with torpedos or mines. Similarly, the field of view of the sensor could be directed inland to gain information on land targets. The great advantage of the infrared imaging sensor is that it will be able to record and transmit, in near real time, evidence of intended hostile activity taking place under cover of darkness perhaps without alerting the enemy that his actions have been observed.

Another mission envisaged for a long-standoff-range, near-real-time infrared imaging device is support for amphibious operations, both vertical and horizontal. The sensor would act like a spotter high in the stands of a football stadium providing timely information on both the offense and the defense.

Other applications include distinguishing friendly forces from enemy forces and near-real-time battle damage assessment. Friendly forces could be marked with insignia or "beacons" that are detectable only in the infrared.

Because the U.S. Navy operates during all seasons and in all parts of the world, it is highly desirable that a Navy imaging sensor be capable of operating satisfactorily over a wide range of environmental conditions. However, since the Navy generally has a number of alternative methods for acquiring information, it is neither necessary nor cost effective that one particular sensor operate satisfactorily

under all circumstances. The purpose of this discussion is to explore the range of performance that a sensor of given design could provide under various environmental conditions to serve as a basis for deciding whether the Navy should pursue the development of such a sensor.

TARGETS

SHIPS

The apparent thermal contrast between a ship and its background is a function of many variables. The actual temperature of its outer surface depends upon the amount of solar energy deposited on the ship, the air temperature, the flow of air past the ship, sea spray, rainfall, and internal heat sources such as the power plant and machinery. Solar heating is the dominant factor in determining ship temperature during the daytime and its influence may persist for several hours after sunset, after which air temperature takes over. The effect of direct solar radiation incident on a ship at any given time is a function of the elevation and azimuth of the sun, atmospheric transmission, cloud cover, and ship heading. In addition, indirect solar radiation, e.g., radiation reflected off the surface of the water and radiation scattered by the clear sky and by clouds contribute to the heat budget of the ship. Because a ship has a large thermal mass, the time history of these factors strongly affects its temperature over a period of several hours. The flow of air past the ship is a function of the speed and direction of both the ship and the wind. Sea spray is a function of sea state and sea direction relative to the ship heading.

Several successful mathematical models[2,3] exist for calculating the ranges at which ships can be detected, classified, and identified by infrared imaging systems as functions of size and orientation of the target, the target-to-background effective temperature difference, atmospheric transmission, and characteristics of the sensor. "Detection," as used herein, is the lowest order task to be performed. When a target is "detected" it may appear as only a hot (or cold) spot or as an ill-defined blob that conveys information only regarding the existence and location of something in the scene. "Classification" is the next higher level of task and is taken here to mean the ability to distinguish warships (combatants) from merchant (noncombatant) ships by characteristic differences in the general outlines of their superstructures. In this discussion, "identification" means the ability to distinguish two ships of a similar class, for example, a Kotlin class destroyer vs. a Forrest Sherman class destroyer.

It has been found[2] that if approximately 66 sensor resolution elements fall on the projected area of a ship, the task of "classification" can be accomplished. If 400

sensor resolution elements fall on the projected area of the ship, "identification" can be performed. For example, for a destroyer class ship having a projected area of 11,500 square feet when viewed from the beam aspect, a ground resolution of about 5.4 feet would satisfy the criterion of "identification." In this context, a resolution element is not simply the geometrical projection of a sensor detector element onto the target but a square (typically) whose edge dimension equals the width of a single bar of a barely resolvable 7-bar MRT target at the same range as the ship and having a temperature difference between adjacent bars equal to the average temperature difference between the ship and its background. "Barely resolvable" implies a 50% probability of performing the task; to achieve a probability of about 96%, the thermal contrast of both the MRT target and the ship should be doubled. (Alternatively, one could maintain the same temperature difference but increase the criterion values for the number of resolution elements falling on the target to about 150 for classification and 950 for identification to increase the probability of performing the task to 96% from 50%.) Thus the ability of a sensor to resolve structural details on a ship (necessary for identification) depends not only on the size of the details but also on their thermal contrasts. Figures 1 and 2 illustrate the increase in information content with increasing numbers of resolvable elements falling on the target.[2]

Ship-to-background temperature difference has been the subject of many studies. MacMeekin and Moser[4] have summarized many of the early results and provided an extensive annotated bibliography. Figure 3, which was adapted from MacMeekin and Moser[4], shows the cumulative frequency of occurrence of effective radiation temperature differences between ships and their backgrounds based on 212 observations comprising spring, summer and fall measurements made at depression angles from 0° to 30° and corrected for atmospheric transmission losses. It is seen that at night, the ship-to-background temperature difference equals or exceeds 5 C° (9 F°) only about 17% of the time. According to these data, if one wants to operate at the 90th percentile at night, one should not assume a ship-to-background temperature difference of greater than about 0.6 C° (about 1 F°). Wilson[5] provides an extensive body of data and a method of computing ship contrast temperatures. Figure 4, from Wilson[5] shows that at the 90th percentile one can expect a seasonally dependent nighttime contrast temperature of about 0.2 to 0.5 C°.

It may be argued that even if the <u>average</u> temperature contrast of a ship were zero, it could still be detectable because some parts would be at higher temperatures and others lower than the average. On the other hand, one shouldn't design an <u>imaging</u> system such that the <u>most intense parts</u> of the target are <u>barely detectable</u>. On the contrary, the design should be geared toward detectability of the <u>least</u> intense parts of the target that are of interest. It is not unusual for the highlights in a

thermal scene to be 100 times as intense as the least intense features that should be detectable if good imagery is to be obtained. Thus the imaging sensor should be able, for example, to display, without saturation, portions of a ship that are, say, 20 C° warmer than the average scene temperature and still display features exhibiting a temperature difference of only 0.2 C°. Furthermore, one should expect an imaging sensor to produce more than just a collection of the most intense hot and cold spots. Although sensor modeling is certainly not an exact science, sensor performance does indeed correlate with average temperature contrast. See, for example, Shumaker et al.[6] One would be at serious risk in designing a system that departs by an order of magnitude from the norms established for successful infrared imaging equipments.

BOATS

In third world conflicts the Navy can expect attacks against its high value ships by small boats. Such attacks may take the form of suicide missions in which a craft like a Zodiac boat is loaded with explosives and propelled at high speed into the side of a ship. The boat presents a very small cross section even for detection and, because of spray, exhibits only a very small temperature difference relative to the water. It is expected that a long-standoff-range infrared imaging sensor would offer its greatest advantage by providing imagery of the boat while it is still tied up at a pier and preparations are being made to launch an attack.

LAND VEHICLES

Gaining useful reconnaissance information about land vehicles may be easier than for boats in some cases and more difficult in others. Acquiring a boat on an imaging sensor is a two-dimensional problem, whereas acquiring a truck on a road is a one-dimensional problem. Similarly, detection of a long series of hot spots along a highway may be sufficient to "identify" a convoy of trucks. On the other hand, a boat at sea can be detected against a quite uniform background ("pure detection") whereas an off-road vehicle must be detected against a competing background ("discrimination detection"). If the land scene contains many non-targets that are very similar in appearance to the target, it may be necessary to satisfy the criterion for identification in order to "detect" the target.[6] Detection of a warm tank situated in a field of warm tank-size boulders may place unanticipated demands upon the sensitivity and resolution of the sensor. If the previously stated criterion for "identification" is applied to a tank in a cluttered environment and if the tank presents a projected area of 250 square feet, a ground resolution of about 0.8 foot

would be required for discrimination detection. That is, identification and detection would be accomplished simultaneously.

The thermal signature of a land vehicle is driven largely by the dynamic process of absorbing solar radiation during daytime and losing heat at night by convection and by radiation to space. Objects of high emissivity and low thermal mass heat rapidly in the sunshine but drop quickly in temperature at night. Similarly, the background goes through a diurnal cycle of warming and cooling that, depending on its thermal and radiative properties, may differ in amplitude and phase relative to a target.

Shen and Ho[7] have provided radiometric temperature data on a static M60 tank which were recorded at Eglin Air Force Base, FL, at half-hour intervals over a 24-hour period on 6 and 7 December 1987. Figure 5 is a plot of some of those data, which were acquired by a calibrated LWIR FLIR, showing temperature of the front of the tank and its grassy background as a function of time. The weather was clear and cloudless with winds ranging from 2 to 11 mph and averaging 6.5 mph. This particular example shows how target and background temperatures track together, with the temperature difference not exceeding 2 C° during the hours of darkness. Figure 6 shows temperature as a function of time for a number of features of the M60 as seen from its front including the hull, turret, track, fender and gun. It is seen that the spread of temperatures is less than 4 C° during early evening hours and it reduces to less than 1 C° in the early morning hours. It should be reiterated that these data are for a static tank; if it had been exercised, larger temperature differences would have existed.

Figures 7 and 8, which were adapted from Nash[8], show the predicted temperature difference between the front of a tank and the background for clear and overcast conditions, respectively, in central Europe. The largest amplitude of about 5 C° (9 F°) occurs in clear weather in the summer time and the smallest amplitude of 0.9 C° (1.6 F°) occurs in overcast winter weather. Note that the tank is warmest relative to its background at about eight o'clock in the evening and coolest within the hour before noon. This rather surprising result occurs because the background temperature varies more rapidly and over a greater range than the tank's temperature. Typically two nulls or crossovers occur each day, in the morning and in the afternoon, at which times the thermal contrast inverts. For this particular situation, the bad things for a high-altitude nighttime imaging sensor occur simultaneously to produce the least ill effect. That is, thermal contrasts are low on overcast nights, when one wouldn't use a high-altitude infrared sensor anyway because of intervening cloud cover.

Figure 9, which was derived from figure 7, shows the number of hours per night that the temperature difference between a tank and its background falls within various half-degree temperature intervals. For example, one can expect the temperature difference to be between 4.5 and 5.0 C° for 3.1 hours of a 10-hour summer night.

Figure 10, which was also derived from figure 7, shows the number of hours per night that any indicated target-to-background temperature difference is exceeded for the front of an army tank in clear weather in central Europe for summer, spring/fall, and winter. It was arbitrarily assumed that for spring/fall, the duration of nighttime was 12 hours, centered at local midnight. Similarly, summer nighttime was taken to be 10 hours long and winter nighttime as 14 hours in duration. If one wanted to develop a sensor capable of imaging such a target for all nighttime hours of clear weather, one should design for a target-to-background temperature difference of 1.3 C° (2.4 F°). On the other hand, because the maximum values of temperature difference are exhibited typically from 1 to 3 hours after sunset, one could optimize performance of the sensor by conducting missions at such times. The above conclusions are subject to the qualification that they are based on a model applied to a certain specific target viewed from the front in clear weather in central Europe.

BACKGROUNDS

EFFECTS OF SCENE TEMPERATURE

The performance of an infrared imaging sensor is dependent not only on the target-to-background temperature difference but also on the absolute temperature of the background. This is true particularly for the mid-wave infrared (MWIR) band, nominally 3 to 5 μm. In this discussion it is assumed that the targets and backgrounds behave effectively as blackbody radiators. The spectral radiant emittance of a blackbody can be calculated by use of Planck's radiation equation and is plotted in figure 11 over the wavelength interval of 2 to 17 μm for temperatures of 260 K, 280 K, and 300 K (8 $^{\circ}$F, 44 $^{\circ}$F and 80 $^{\circ}$F, respectively). Note that, as the temperature is reduced, the peak value decreases and the distribution shifts to longer wavelengths. For the present situation, the band of interest is that between 3.4 and 5.0 μm. The small areas under each of the curves in this band represent the relative amounts of power available to the sensor at those different temperatures. For a temperature of 300 K, the integrated radiant emittance is more than five times greater than for a temperature of 260 K. In terms of photon emittance, the numbers of photons emitted per square centimeter per second by a

blackbody at temperatures of 260, 280, and 300 K are 2.516×10^{15}, 6.025×10^{15}, and 1.290×10^{16}, respectively. For a photon-counting detector, the disadvantage of operating at the lower scene temperatures is partially off set by an decrease in background radiation noise, which varies as the square root of the number of photons received.

It can be seen from figure 11 that the MWIR band is particularly vulnerable to decreases in scene temperature because the blackbody radiation curve shifts toward longer wavelengths as the temperature is reduced. For most current FLIRs and line scanners, which operate in the long-wave infrared (LWIR) band (nominally 8 to 13 μm), the decrease in available radiant power with decreasing scene temperature is not nearly as great. For the LWIR band, there is a compensating factor of improved atmospheric transmission at low temperature because of the typical concomitant reduced water vapor concentration. Furthermore, in the LWIR band the decrease in sensitivity is usually ignored because ample sensitivity is generally available. Such would not be the case for a MWIR system that exhibits, at best, marginal sensitivity at high scene temperatures.

In an infrared imaging sensor, one is more interested generally in small differences in effective temperature rather than actual temperature values. To illustrate this point, figure 12 shows basically a view of the portions of the curves of figure 11 expanded to cover only the spectral region from 3.2 to 5.2 μm. However, upon closer examination, it is seen that each of the earlier curves has been replaced by two curves, corresponding to a temperature difference of 1 C° centered about the earlier curves. For example, the upper two curves are the spectral radiant emittances for temperatures of 300.5 K and 299.5 K, and the narrow sliver bounded by these two curves between the wavelength limits of 3.4 and 5.0 μm represents the "signal" available from a target that differs by 1 C° in temperature from its background at a mean reference temperature of 300 K. For the other two pairs of curves, the enclosed sliver areas correspond to 1 C° differences at mean reference temperatures of 280 K and 260 K. By comparing these three pairs of curves, one can see how the "signal" (sliver area) decreases as the reference (background) temperature is reduced.

In figure 13, the differences (i.e., the sliver heights) between the curves in each of the three pairs of curves in figure 12 have been plotted on an expanded vertical scale. If one has a sensor that responds uniformly over the wavelength interval 3.4 to 5.0 μm and if the atmospheric transmittance is uniform over that band, then the signal generated by the detector will be proportional to the area under each of these curves. These integrated values, in units of $\mu W \cdot cm^{-2} \cdot K^{-1}$, are 20.55, 10.88, and 5.20 for background temperatures of 300, 280 and 260 K,

respectively. Relative to a background temperature of 300 K, temperatures of 280 and 260 K enable "signals," for a 1 K difference in temperature, that are 53% and 25% as great, respectively. In other words, to a very good approximation, at a background temperature of 260 K (8.3°F), a 4-K temperature difference is needed to produce the same signal as a 1-K difference at a background temperature of 300 K (80.3°F). Figure 14 shows how, because of this factor, the relative signal varies with background temperature over the range of -40°F to 100°F. The curve of figure 14 is normalized to unity for a reference temperature of 300 K. In general, a MWIR imaging sensor will perform significantly better in the tropics than in the arctic. Consequently, Hawaii is a favorite place to conduct tests.

TEMPERATURE STATISTICS FOR MARINE AREAS

To determine the potential significance of the foregoing to an operational system it is necessary to inquire where and when the Navy might want to operate the sensor and to review the temperature statistics for those situations. Air temperature data for many marine areas were readily available to the author in the form of tables in publications of the U.S. Naval Weather Service Command[9].

To illustrate the kind of data that are available, figure 15 is provided as an example of the annual distribution of air temperature based on 7491 day and night observations made during the primary period of 1909 to 1968 for "New York," the marine area bounded by 40° north latitude and the coast and 72° west longitude and the coast. Figure 16 shows the cumulative distribution of temperature for the same data as figure 14. From the graph one can see, for example, that the temperature is less than 40°F about 16% of the time, day and night, over the whole year.

To arrive at a somewhat broader statistical base, twenty northern hemisphere maritime sites were selected as being representative of the types of climate in which future naval operations might be expected to take place. These are listed in table 1 and their locations are shown on the map of figure 17. It may appear that a disproportionately large number of the sites are in the lower latitudes; however, these are the sorts of places where wars seem to break out. Even though, in many cases, the sites are identified by names such as "Boston" and "Matsue," it must be remembered that the data pertain to maritime areas adjacent to such places and not necessarily to a city itself. Indeed, the highs and lows of temperature experienced over the ocean are significantly less extreme than those observed over the nearby land, particularly for places located near the eastern coastlines of continents (because prevailing winds are typically westerly).

Means, extremes, and percentiles of temperature by three-hour intervals (0000-0300 GMT, 0600-0900 GMT, 1200-1500 GMT and 1800-2100 GMT) were taken from publications of the Naval Weather Service Command and plotted as figures 18 through 37.

It is interesting to note that for these maritime areas, temperatures vary fairly little (typically of the order of 5 F°) as a function of time of day. This is attributable to the fact that the atmosphere, being quite transparent to solar radiation, absorbs very little energy directly; the bulk of the radiation penetrates the ocean where most of it is absorbed over the first few hundred feet of depth. Because the specific heat capacity of water is very high and because the radiation is absorbed over a significant thickness of water, the temperature rise is small. The over-land situation is quite different. Soil is quite opaque, is often dark in color and therefore a strong absorber, is a poor heat conductor, and has a lower specific heat capacity than water. Therefore solar radiation is strongly absorbed near its surface where it produces a large rise in temperature. The warm soil then heats the adjacent air indirectly.

As stated previously, in the discussion of ship targets, air temperature is the primary driver of hull temperature following a cool-down period which occurs a few hours after sunset. Wilson[5] provides a method for computing ship temperatures consisting of determining what its temperature would be based on environmental effects and applying "corrections" for internal sources of heat and certain construction features. For the present purposes, it is adequate to assume that the hull will be at about the ambient air temperature and that the hull will serve as a background against which warm spots, such as the engine areas, will be imaged. If one takes, as a specific example, the marine area near New York, (figure 22) one notes that about 99% of the time the air temperature will be about 20 $^{\circ}$F or higher and that 95% of the time it will be about 30 $^{\circ}$F or higher. Thus, if one wants to develop a sensor that will not be limited by low background temperature more than 1% of the time in the New York area, one should assume a value of 20 $^{\circ}$F (-6.7 $^{\circ}$C, 266.5 K).

To arrive at a "world-wide" (i.e., 20 selected maritime sites) distribution of nighttime temperatures, a subset of the data used in preparing figures 18 through 37 was used to prepare figure 38. For each of the 20 areas, one curve corresponding to a 3-hour nighttime interval was selected. For example, for New York, the interval 0600-0900 GMT, corresponding to 0100 to 0400 eastern standard time, was selected and the temperatures corresponding to the 99th, 95th, 50th, 5th and 1st percentiles were plotted for the latitude of 40.4 $^{\circ}$ north. This process was repeated for the other 19 sites, resulting in five line graphs of temperature vs. site latitude. Figure 38 shows that to cover the full gamut of nighttime marine air temperatures for the 20 sites at

the 99th percentile, one should plan on encountering temperatures as low as 18°F (-7.7°C, 265.4 K).

The ship background may be the sea surface, sky, land, or a combination of these. The reflectivity of smooth sea water varies as a function of viewing angle, ranging from about 2% normal to the surface and increasing slowly to about 6% at an angle of 60° relative to the normal and then increasing to 100% at a grazing angle. However, the sea surface is rarely perfectly smooth and the effect of waves is to reduce the reflectivity. If the surface were perfectly smooth, the sea surface would appear to merge continuously into the sky and one would not be able to see the horizon because the sea would behave as a perfect mirror near the horizon. In reality, because of multiple reflections from waves, the reflectivity increases with angle to a maximum of only about 25% and reaches this peak value at an angle of about 80°.

To an infrared sensor, the apparent temperature of a clear sky varies dramatically with viewing angle, ranging from very low values (of the order of -40°C, depending on wave band) near zenith (in which case the path length through the atmosphere has its minimum value and one is essentially looking out into the void of space), to values close to the air temperature at sea level when one is viewing along a horizontal path through the maximum amount of the most dense part of the atmosphere. Thus, if one is viewing a ship from low altitude over a horizontal line of sight, the ship will be viewed against a sky background of effective temperature that is close to the sea level air temperature.

If a ship is viewed against a sea background, the situation becomes more complicated insofar as what one sees is a combination of radiation emitted by the sea (and therefore characteristic of the sea temperature) and radiation emitted by the sky and reflected off the water. For an opaque body (as is water in the infrared part of the spectrum) the ability of a surface to emit radiation is governed by its absolute temperature (raised to the fourth power) and its emissivity, which equals one minus the reflectivity. Thus, for viewing conditions in which the reflectivity is low (e.g., looking straight down at the sea surface), the emissivity is close to its maximum value of one (i.e., about 0.98) and the radiation detected is mostly that emitted (rather than reflected) by the surface. In such a situation, the apparent temperature of the background against which a ship is viewed is very close to the actual surface temperature of the water. On the other hand, if the ship is viewed under clear sky conditions at an angle of 80° relative to the normal (10° depression angle), the sea background will appear considerably cooler and the ship hull, which might have appeared cool relative to the sea background when viewed vertically, might now appear warm relative to its background. If clouds are present,

particularly in the form of a continuous ceiling of low altitude clouds, the apparent sea surface temperature will be higher but the variation with viewing angle will be much smaller.

TEMPERATURE STATISTICS FOR A LAND REGION

Biberman[10] and his associates have compiled a significant body of data on weather conditions at Hannover, Germany, and the effects of weather on electro-optical imaging devices. Figures 39, 40, 41 and 42 were adapted from Biberman and show the hourly readings of air temperature and dew point for the entire year 1970. For the months of May, June, July and August, when clear weather prevails, diurnal variations of the order of 10 C° (18 F°) occur. Typically, at night the air temperature decreases to the dew point. During the winter months, when cloud cover and poor visibility prevail, the diurnal variation is not evident and the air temperature rarely rises more than a few degrees above the dew point.

From the foregoing it is concluded that the recorded values of dew point represent a reasonably good measure of nighttime temperature (for Hannover, Germany). Figure 43, which is also from Biberman[10], shows the fraction of the hourly readings for which the dew point did not exceed the indicated temperatures for all of 1970. This curve of cumulative frequency of occurrence shows that the dew point is less than or equal to -6.9°C (19.6°F, 266 K) 5% of the time, and less than or equal to -10.7°C (12.7°F, 262 K) 1% of the time.

The preceding discussions, although limited to a relatively few selected sites, seem to indicate that requiring an infrared imaging sensor to operate satisfactorily for scene background temperatures of the order of 260 K would be appropriate for possible future U.S. Navy applications.

CLOUD CEILING

Another factor that limits the satisfactory use of airborne, air-to-surface, imaging devices operating in the visible or infrared parts of the spectrum is intervening cloud cover. The sensor is constrained to operate below any ceiling that might exist in the area of interest. It is desirable to operate with a cloud-free line of light between the sensor and the surface. Indeed, even an occasional small cloud within the sensor's field of view might make the entire image useless.

Publications of the Naval Weather Service Detachment, Asheville, NC, [11,12] provide a large body of synoptic cloud ceiling information for scores of maritime areas throughout the world. A "ceiling" is considered to exist if the cloud cover at any given altitude is equal to or greater than 5/8. Data were selected for sites in the Yellow Sea, Norwegian Sea, Atlantic Ocean east of the Azores, and Mediterranean Sea and plotted in figures 44, 45, 46, 47, and 48 as frequencies of occurrence and as cumulative frequencies of occurrence for the months of January and July. These curves show the probability that a cloud ceiling will exist below any indicated altitude up to 8000 feet.

To the extent that the data from these five sites may be considered representative, the message is quite clear. That is, except for the two selected sites in Mediterranean Sea, the probability of having a ceiling at or below 8000 feet is of the order of 50%. Of the ten locations/times examined, the best for high altitude reconnaissance is the eastern Mediterranean in July for which a low cloud ceiling exists only about 3% of the time. Clouds over the oceans occur most frequently in the altitude regime of 1000 to 3500 feet; accordingly, flying at 6000 feet vs. 8000 or 40,000 feet doesn't improve the odds significantly. If one wants a system that will not be limited by cloud cover, say, 90% of the time, one should insure that the selected design be consistent with an operating altitude of the order of 1000 feet. (This "requirement" will introduce a need for greater thermal sensitivity for the equipment than for one that would operate less frequently but at significantly higher altitudes because of the greater atmospheric attenuation that occurs over long, low-altitude paths.)

VISIBILITY

Visibility is another environmental factor that must be included in calculations of system performance. Visibility is a function of the number and size of aerosol particles in the atmosphere and is usually measured in the visible part of the spectrum (as the term implies) over a low-altitude horizontal path. Scaling rules have been established to permit extrapolation of "visibility" to the infrared bands. Transmission is generally affected less adversely by aerosols in the infrared bands than in the visible. Furthermore, if one is viewing the surface from high altitude, the effects of aerosols may not be as bad as one might expect, because the aerosol layer, which tends to be concentrated at the low altitude where visibility is measured, occupies only a small portion of a long viewing path.

Visibility data for marine locations are provided in the same sources as the cloud ceiling data.[11,12] Reduction of these data to a convenient graphical form is

beyond the scope of this quick-look study. However, a sample of processed data from Biberman[10] is given in figure 49. For all of 1970 in Hannover, Germany, the visibility was less than or equal to 7.3 km (3.9 nmi) 50% of the time. Ten percent of the time, the visibility was less than 0.9 km (0.5 nmi).

PRIOR WORK / LONG FOCAL LENGTH IMAGING DEMONSTRATION PROJECT

Before one embarks on a new development effort it is appropriate to review what has been done previously. Perhaps the most relevant prior project was the "Long Focal Length Imaging Demonstration" (LFLID)[13,14] project which was pursued by the Navy in the early 1980s and culminated in a demonstration of an MWIR sensor mounted at the summit of Mount Haleakala, Maui, HI, during June 1984. Key characteristics of this sensor are summarized in table 2 along with those of the currently proposed Loral Fairchild Systems IREO LOROPS.

The LFLID project was undertaken to demonstrate technologies applicable to a standoff infrared imaging equipment for the long-range oblique reconnaissance application of passively detecting tactical vehicles and recognizing ships under day/night unobscured conditions at ranges of at least 30 nmi. Prior studies included definition of an approach for stabilizing the optical system in a reconnaissance aircraft.[15] However, because the development of even a brassboard-level flyable equipment would have been prohibitively expensive, it was decided to fabricate a sensor suitable for ground-based use and to operate it in a fixed mode on a mountain top to produce a long slant path to the surface from an altitude of 10,000 feet to simulate in part airborne operation of the sensor.

The LFLID sensor was used to image ships, vehicles, and buildings at various ranges. Most of the data were acquired during hours of darkness although some imagery was produced as late as 0930 local time. An LST was acquired at a range of 30 nmi and tracked out to 71 nmi where it was lost behind clouds. It was said to be recognizable at 35 nmi and detectable as a white spot at 71 nmi. The best-looking ship imagery was obtained while viewing sunlit ships in a general westerly direction within several hours after sunrise. Hess et al.[14] provide recognizable images of a guided missile cruiser recorded at a distance of 18 nmi at 0908 and a cruiser at a range of 20 nmi at 0717 local time.

Imagery of three National Guard vehicles (a jeep, a 2.5-ton truck, and a Gamma Goat personnel carrier) and a civilian automobile at a 3500-ft altitude site 7.1 nmi away permitted discrimination among vehicle types and detection of

individual personnel. At a sea level site 12 nmi away, it was possible to detect each of the vehicles and barely to discriminate among them, as well as to detect movement of the group of personnel. Vehicles were detectable at a range of 16 nmi, aided by their motion. At 29 nmi, the truck was detectable but it probably could not have been distinguished from ground clutter had its presence not been cued by a nearby highway flare.

The originally predicted noise-equivalent temperature difference (NETD) for the LFLID equipment was 0.033 C°. As development proceeded, the predicted value degraded to 0.09 C°. When NETD was measured, an even poorer value of 0.5 C° was obtained. For the demonstration, the effective NETD was improved by use of 64-line averaging to 0.07 C°; however, this was accomplished by increasing the time required to scan out a frame to about 6 s from about 0.09 s. It was possible to increase the "exposure time" to such a large value because the equipment was mounted at a fixed site and was viewing targets moving at low angular velocity relative to the sensor. Several messages may be drawn from the foregoing: (1) Performance parameters can often be traded off to achieve improved performance under a given (but restricted) set of circumstances. (2) An NETD of the order of 0.07 C° (corresponding to MRT $\leq$ 0.5 C° for spatial frequencies $\leq$ 20 cycles/mrad) is necessary to produce recognizable ship imagery at ranges up to about 35 nmi under favorable conditions (tropical environment, very clear atmosphere, sensor rigidly mounted at 10,000-ft altitude). (3) The performance of developmental model equipments often falls short of theoretical expectations.

SENSITIVITY REQUIREMENTS

Successful infrared line scanners (IRLS) and forward looking infrared (FLIR) imaging devices have exhibited values of noise equivalent temperature difference (NETD) in the range of 0.1 to 0.2 C°. An IRLS, typically, operates over a relatively short, nearly vertical viewing path through the atmosphere (of the order of several thousand feet); consequently, signal loss in the atmosphere is generally small. On the other hand, a Navy FLIR is generally used for viewing targets over longer, nearly horizontal paths (of the order of two to ten nautical miles) for which atmospheric attenuation can be quite significant. Because most U.S. FLIRs produce imagery at the rate of 30 frames per second, and the human eye integrates over about 0.2 second (i.e., it integrates over 6 frames), an increase in effective signal-to-noise ratio of $6^{1/2} = 2.4$ is achieved. This increase in effective sensitivity tends to compensate for the longer attenuating paths over which a FLIR operates relative to an IRLS.

The IREO LOROPS is planned to operate over ranges of about 20 miles but over paths from high altitude that do not attenuate as severely (per mile) as typical low-altitude FLIR paths. Because the frame rate of IREO LOROPS is only about 1% as great as that of a FLIR there is little opportunity for improvement of effective signal-to-noise ratio by frame-to-frame integration. Thus, to achieve imagery (at long stand-off range) of quality comparable to that achievable by an IRLS and a FLIR in their normal operating modes, IREO LOROPS should provide a noise-equivalent temperature difference in the range of 0.05 to 0.1 C°. A convenient rule of thumb for a well-designed FLIR is that the minimum resolvable temperature difference (MRT) at its "nominal resolution" (Nyquist frequency or half the cutoff frequency) equals 2.7 times the NETD. For a single-frame device (such as an IRLS or IREO LOROPS) another factor of $6^{1/2}$ is introduced. Therefore, for the IREO LOROPS under laboratory conditions, the MRT at the Nyquist frequency should be in the range of 0.33 to 0.66 C°.

IREO LOROPS SENSITIVITY CALCULATIONS

The sensitivity of an infrared imaging equipment can be calculated by use of radiant power or radiated photons. Traditionally, the performance of mechanically scanned FLIRs and IRLSs has been reckoned in terms of detectivity D^* (a measure of detector sensitivity in terms of power), which is useful for systems with discrete detectors producing continuous, unsampled output waveforms. For staring-type imagers, in which two-dimensional arrays of many thousands of detector elements with discrete charge storage sites are used, the signal can be expressed conveniently in terms of charge carriers (electrons or holes) stored in a sampling site over the integration period. Performance measures have been derived by Moser and MacMeekin[16] in terms of power and by Campana[17] in terms of photons. Because the IREO LOROPS is a hybrid device (i.e., it is a mechanically scanned device that uses discrete storage sites) and because a check on the results was desired, calculations were done by both methods. As an additional check on the method, an NETD calculation was performed for the LFLID equipment based on data given in table 2. The calculated NETD was in close agreement with the measured NETD of 0.5 C°.

Calculations of NETD and MRT (at the Nyquist frequency) were performed for the IREO LOROPS for scene temperatures of 260, 280, and 300 K using Loral Fairchild Systems design data.[18] It was assumed that the two-dimensional array consisted of 48,000 PtSi detector elements set on a pitch of 40 x 40 μm with 75% fill factor, corresponding to an active area per detector element of 0.000012 cm^2. For InSb, a staggered linear array of 3000 InSb detector elements on a pitch of 40 μm

was assumed and two sizes of detector elements were considered: 40 x 40 μm and 50 x 50 μm. Values of quantum efficiency of 0.007 and 0.95 were assumed for PtSi and InSb, respectively. It was further assumed that the internal temperature of the sensor was 300 K (independent of scene temperature) and that for a scene temperature of 300 K, only 22% of the photons that were incident on the detector originated from the scene while most originated within the sensor itself. These values were scaled for other scene temperatures such that for 280 K, only 12% of the photons were from the scene and for 260 K, only 5% were from the scene. Because such a large fraction of the photons, which contribute nothing in the way of signal but produce noise in proportion to the square root of their number, originate within the sensor, the noise remains at a high level even when low-temperature scenes are viewed. (Ideally, only scene photons should impinge on the detector.) Thus, when low-temperature scenes are viewed, there is a significant decrease in signal photons but not in noise photons.

The results of the calculations for the three detector arrays and for three scene temperatures are given in table 3. It is seen that the NETD bogey in the range of 0.05 to 0.1 C° (MRT of 0.33 to 0.66 C° at the Nyquist frequency) is not achievable with the proposed PtSi array at any of the three scene temperatures. Also, for a scene temperature of 260 K, neither InSb detector array meets the goal. However, the InSb array with 50- by 50-μm elements exceeds the goal for scene temperatures of 280 K and 300 K while the InSb array with elements of sensitive area of 40- by 40-μm exceeds the goal only for a scene temperature of 300 K but does come close for 280 K.

CONCLUSIONS

A long-standoff-range MWIR imaging sensor capable of being used successfully by the Navy against a variety of sea and land targets should be designed to operate under the following target, environmental, and operational conditions:

► The sensor should be designed to accommodate target-to-background temperature differences (averaged over the target) of 0.5 C°. The dynamic range of the sensor should match the range of intra-target temperatures (after accounting for atmospheric propagation losses) such that the most intense features do not saturate the system and the smallest temperature differences of interest are barely detectable (as opposed to the most intense features being barely detectable). To enable this level of performance, the sensor should provide, under laboratory conditions, an NETD in the range of 0.05 to 0.1 C°.

► The sensor should be designed to yield the above sensitivity for scene background temperatures over the range of 260 K to 300 K.

► Because of the frequency of low cloud ceilings, the sensor should be capable of proper operation at altitudes as low as 1000 feet. Such operation may impose more rigorous demands upon equipment sensitivity insofar as atmospheric attenuation is most severe for low-altitude, near-horizontal paths. In addition, because of increased buffeting at low altitude, the stabilization system will have to accommodate greater levels of platform unsteadiness.

► The sensor should be capable of proper operation for visibility (measured over a near-sea-level horizontal path) as low as 5 km.

The proposed IREO LOROPS[18] will not satisfy the above "requirements." A staggered linear array of 3000 "oversized" (50 by 50 μm) InSb detectors would enable the sensor to satisfy the "requirements" for a majority but not all of the situations considered. If the number of photons that originate within the sensor itself and impinge on the detector array could be reduced by an order of magnitude, the sensitivity goal could be achieved for scene temperatures of 260 K. Redesign of the pencil mirror and/or perhaps cooling it might ease the problem.

Elimination of the need for 16 stages of time delay and integration will ease the problem of stabilization of the sensor to being less severe than for when the sensor is operating in the visible part of the spectrum.

ACKNOWLEDGEMENT

Special appreciation is extended to Mr. Chyau N. Shen of NAVAIRWARCENACDIVWAR and Dr. John Y. Ho of CNV&EO for providing target temperature data used in preparing figures 5 and 6.

REFERENCES

1. National Research Council, Naval Studies Board "Implications of Advancing Technology for Naval Warfare in the Twenty-First Century" (Navy-21 Study)

2. P. M. Moser, "Mathematical Model of FLIR Performance," Naval Air Development Center Technical Memorandum NADC-20203A:PMM, AD-A045247, 19 October 1972

3. A. H. Blumenthal and S. B. Campana, "Development of an Aperiodic Electro-Optic Image Quality Model for Ship Target Discrimination," Naval Air Development Center Independent Research Task No. R0112, Work Unit No. GC110

4. N. E. MacMeekin and P. M. Moser, "Ship-to-Background Temperature Differences," Naval Air Development Center Technical Memorandum NADC-20203:NEM/PMM, AD-C012453, 16 September 1974

5. D. M. Wilson, "A Method of Computing Ship Contrast Temperatures Including Results Based on Weather Ship J Environmental Data," Naval Surface Weapons Center Report NSWC/WOL TR 78-187, AD-A078794, 29 January 1979

6. D. L. Shumaker, J. T. Wood and C. R. Thacker, "FLIR Performance Handbook," DCS Corporation, Alexandria, VA 22314

7. C. N. Shen, Naval Air Warfare Center, Aircraft Division Warminster, and J. Y. Ho, Center for Night Vision & Electro-Optics, Private communication

8. C. J. Nash, "Visionics Handbook Sensitivity Analysis," Report to U. S. Army Night Vision and Electro-Optics Laboratory (DELNV-V), October 1980

9. U. S. Naval Weather Service Command, "Summary of Synoptic Meteorological Observations, North American Coastal Marine Areas, Volume 2 (Boston, Quonset Point, New York, Atlantic City), AD-707699, May 1970 (This is one of many similar volumes in a series.)

10. L. M. Biberman, "Effect of Weather at Hannover, Federal Republic of Germany, on Performance of Electrooptical Imaging Systems, Part 1. Theory, Methodology, and Data Base," Institute for Defense Analyses Paper P-1123, August 1976

11. U. S. Naval Weather Service Command, "U. S. Navy Marine Climatic Atlas of the World, Volume I, North Atlantic Ocean, NAVAIR 50-1C-528, December 1974

12. U. S. Naval Weather Service Command, "U. S. Navy Marine Climatic Atlas of the World, Volume II, North Pacific Ocean, NAVAIR 50-1C-529, Revision of March 1977

13. M. R. Hess, W. K. Hull and M. D. Gibbons, "Long Focal Length Imaging Demonstration," Proceedings of the IRIS Specialty Group on Infrared Imaging, January 1984

14. M. Hess, J. Gibbons, J. Toner, W. Abrams, R. Chin, M. Gibbons, and M. Winn, "The Long Focal Length Imaging Demonstration (LFLID) Project," Proceedings of the IRIS Specialty Group on Infrared Imaging, March 1985

15. Y. Shaham, D. Stites, J. Melzer, and C. Perrygo, "Analysis of High Performance Telescope for Airborne Environments," Proceedings of the IRIS Specialty Group on Infrared Imaging, December 1981

16. P. M. Moser and N. E. MacMeekin, "Index of Performance for FLIR (Forward Looking Infrared) Imaging Devices," Naval Air Development Center Report No. NADC-72167-AE, AD-525116, 10 April 1973

17. S. B. Campana, "Second Generation FLIR Performance Summary Measures," Naval Air Development Center Technical Memorandum NADC-3011:SBC, 17 September 1979

18. Loral Fairchild Systems Review Draft of Final Report "DoN EO-LOROPS Image Sensor IR Retrofit, AN/AVD-5 IR Upgrade Evaluation," 13 January 1992

Table 1. SELECTED REPRESENTATIVE MARITIME SITES

MAP CODE	LATITUDE	LONGITUDE	SITE DESCRIPTION
A	56 N-Coast	151-157 W	Kodiak, AK (NE Pacific Ocean)
B	51-55 N	172-180 W	Adak, AK (NE Pacific Ocean)
C	45-47 N	53-56 W	Argentia, Newfoundland (Atlantic Ocean SE of Newfoundland)
D	42 N-Coast	66 W-Coast	Boston, MA (Atlantic Ocean E of central MA)
E	40 N-Coast	72 W-Coast	New York, NY (Atlantic Ocean S of Long Island)
F	39.7 N	129.4 E	Wonsan, North Korea (Sea of Japan)
G	38-40 N	72 W-Coast	Atlantic City (Atlantic Ocean E of NJ, MD and DE)
H	37.9 N	25.1 E	South Aegean Sea (E of Athens, Greece)
I	36-38 N	126 W-Coast	San Francisco, CA (Pacific Ocean S and W of central CA)
J	36.0 N	3.4 W	Malaga, Spain (W end of Mediterranean)
K	36.0 N	133.2 E	Matsue, Japan (S end of Sea of Japan)
L	32.2 N	33.3 E	Port Said, Egypt (SE Mediterranean)
M	27.2 N	50.2 E	NW Persian Gulf (between Saudi Arabia and Iran)
N	25.0 N	57.8 E	N Gulf of Oman (between Iran and Oman)
O	22.9 N	67.8 E	Karachi, Pakistan (N Arabian Sea)
P	20.4 N	158.3 W	Hawaiian Leeward (Pacific Ocean S of Oahu)
Q	18.3 N	107.5 E	Tonkin Gulf (E of N Vietnam)
R	18-20 N	74-76 W	Guantanamo, Cuba (Caribbean S of E Cuba)
S	17.9 N	85.2 E	Vishakhapatnam, India (Bay of Bengal E of S India
T	14.2 N	73.0 E	Panjim, Goa (Arabian Sea W of S India)

Table 2. DESIGN AND PERFORMANCE CHARACTERISTICS OF TWO LONG FOCAL LENGTH INFRARED IMAGING SENSORS

CHARACTERISTIC	LFLID	IREO LOROPS
Focal Length (cm)	180.98	167.64
Aperture Diameter (cm)	50.0	30.48
Focal Ratio	f/3.62	f/5.5
Wave Band (μm)	3.5 - 5.1	3.4 - 5.0
Detector Material	InSb	PtSi
Number of Detector Elements	512	48,000 (3000 x 16 TDI stages)
Field of View (mrad)	10.1(V) x 10.8(H)	71.58 x 71.58 (variable)
Detector Element Angular Subtense (μrad x μrad)	28 x 28	23.86 x 23.86 (?)
Size of Detector Elements (μm x μm)	48 x 48	40 x 40 (?)
Detectivity D* ($cm \cdot Hz^{1/2} \cdot W^{-1}$)	4×10^{11}	?
Optics Tranmission (%)	50 (predicted) 12.5 (measured)	79 (?)
NETD (C°)		
calculated	0.033, 0.09	
measured	0.5	
measured with 64-line averaging	0.07	
Predicted MTF	0.3 at 29 cy/mrad	
MRT (C°)		
calculated	0.3 at 20 cy/mrad	
measured	0.2 at 15 cy/mrad	
Active Scan Time Per Frame (s)	0.092	3 (?)

Table 3. PREDICTED SENSITIVITY OF IREO LOROPS AS A FUNCTION OF DETECTOR ARRAY AND SCENE TEMPERATURE

Detector Array	Scene Temperature (K)					
	260		280		300	
	NETD	MRT*	NETD	MRT*	NETD	MRT*
3000 x 16 PtSi elements each 0.000012 cm^2 in sensitive area	0.73	4.83	0.35	2.33	0.19	1.24
3000 x 1 InSb elements each 0.000016 cm^2 in sensitive area	0.22	1.44	0.10	0.69	0.055	0.37
3000 x 1 InSb elements each 0.000025 cm^2 in sensitive area	0.17	1.15	0.083	0.55	0.036	0.29

* at Nyquist frequency

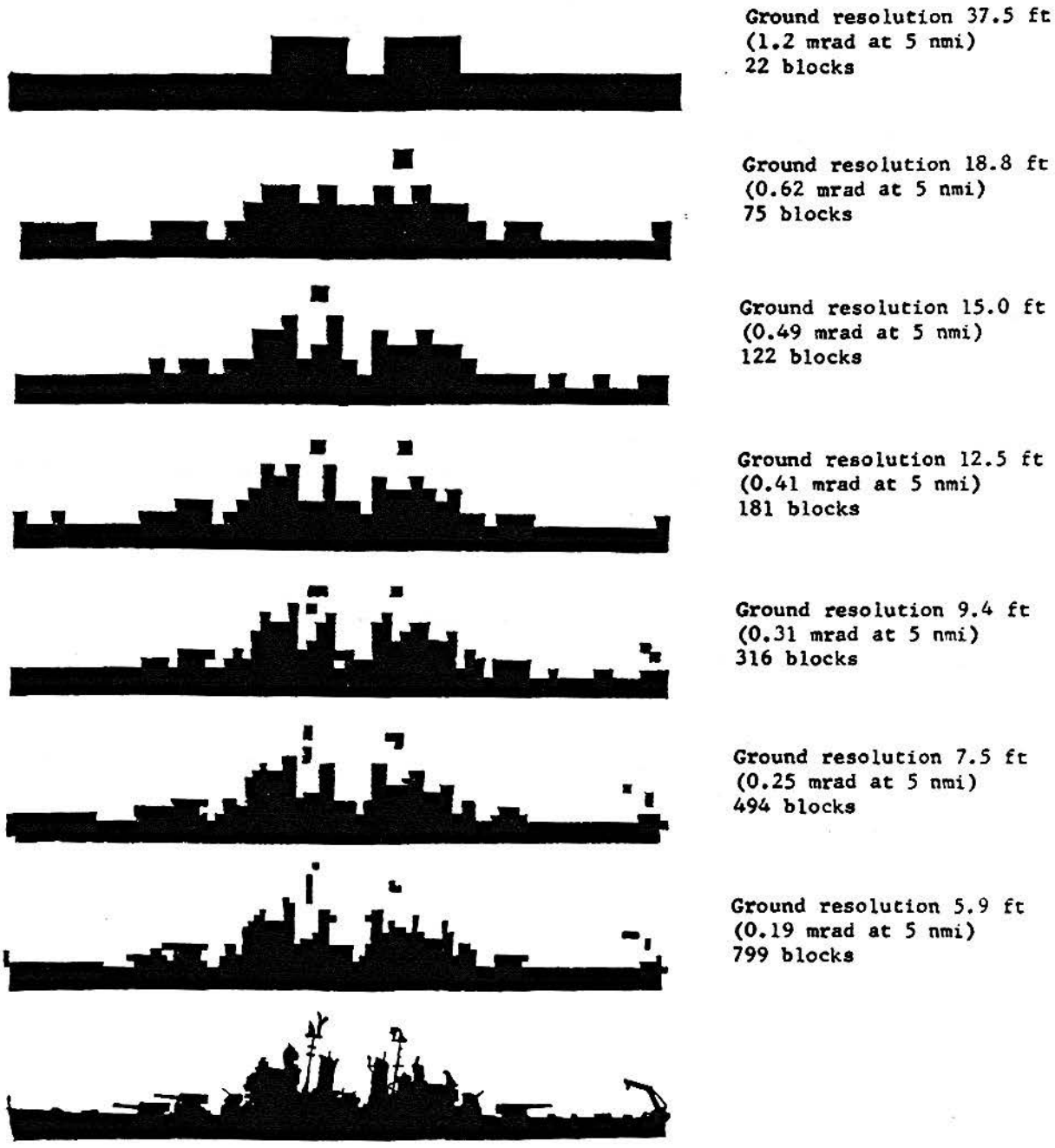

Figure 1. Block-type and graphic profile silhouettes of a Baltimore class heavy cruiser[2]

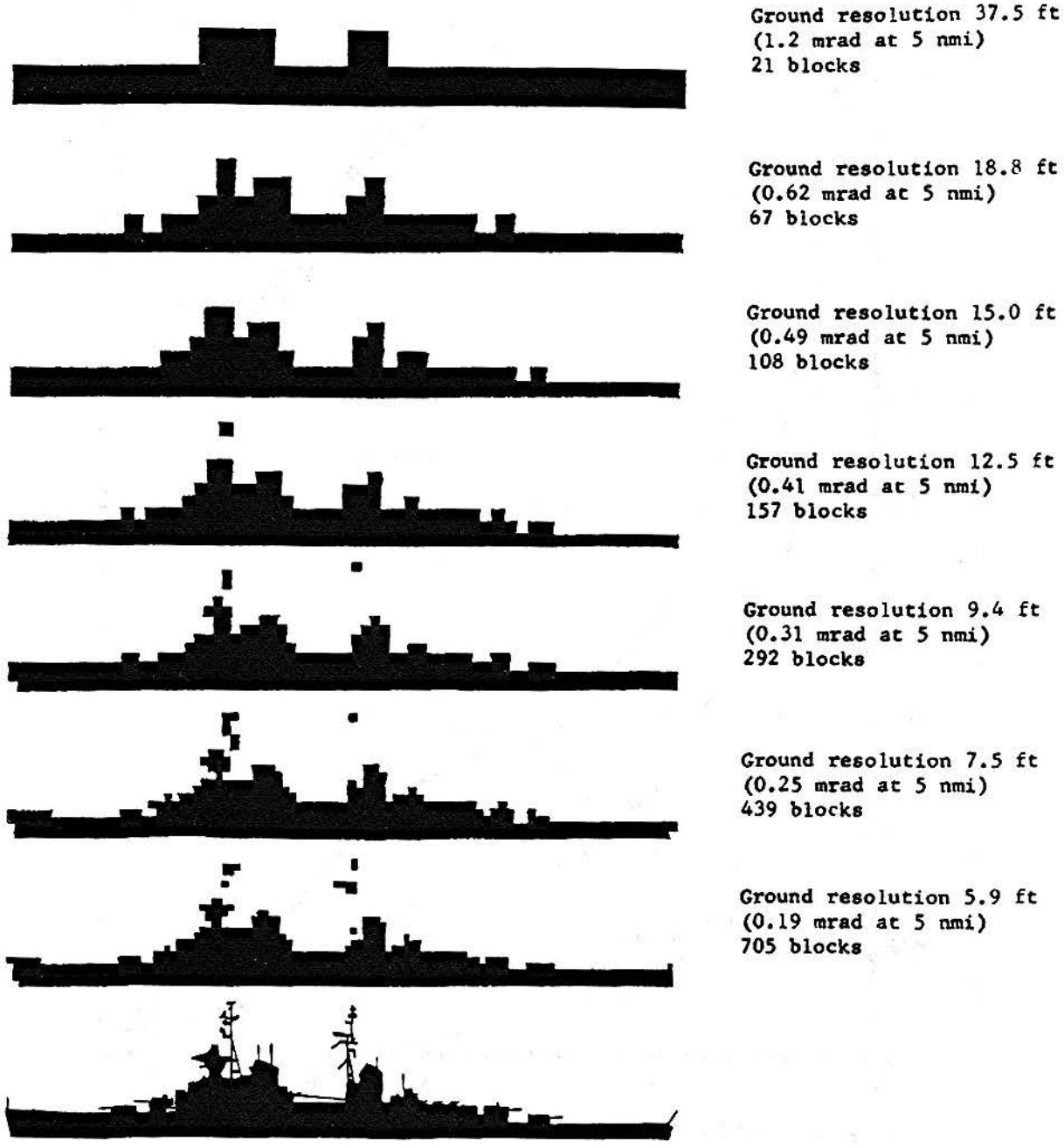

Figure 2. Block-type and graphic profile silhouettes of a Sverdlov class cruiser[2]

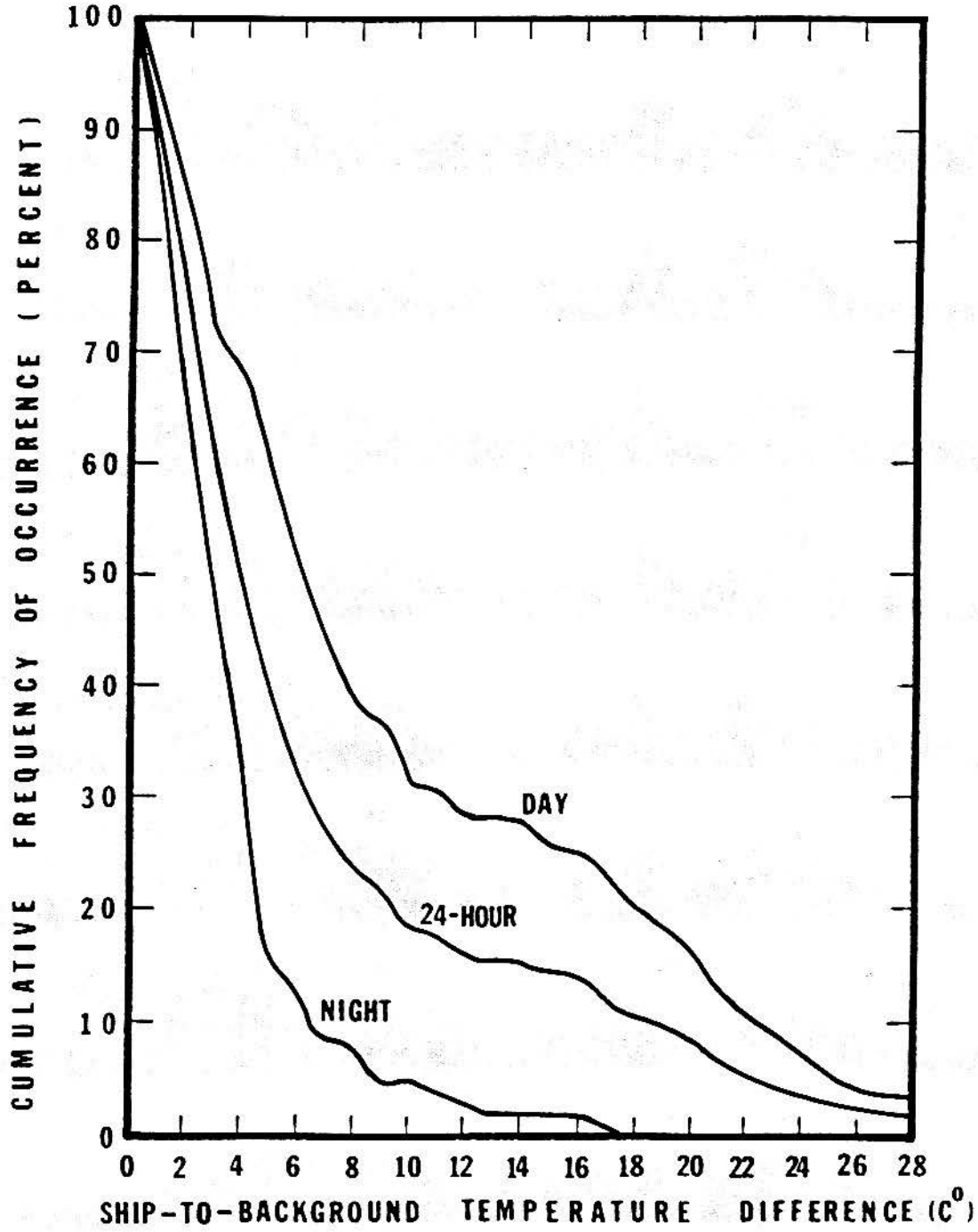

Figure 3. Probability that the temperature difference between a ship and its background will exceed indicated values[4]

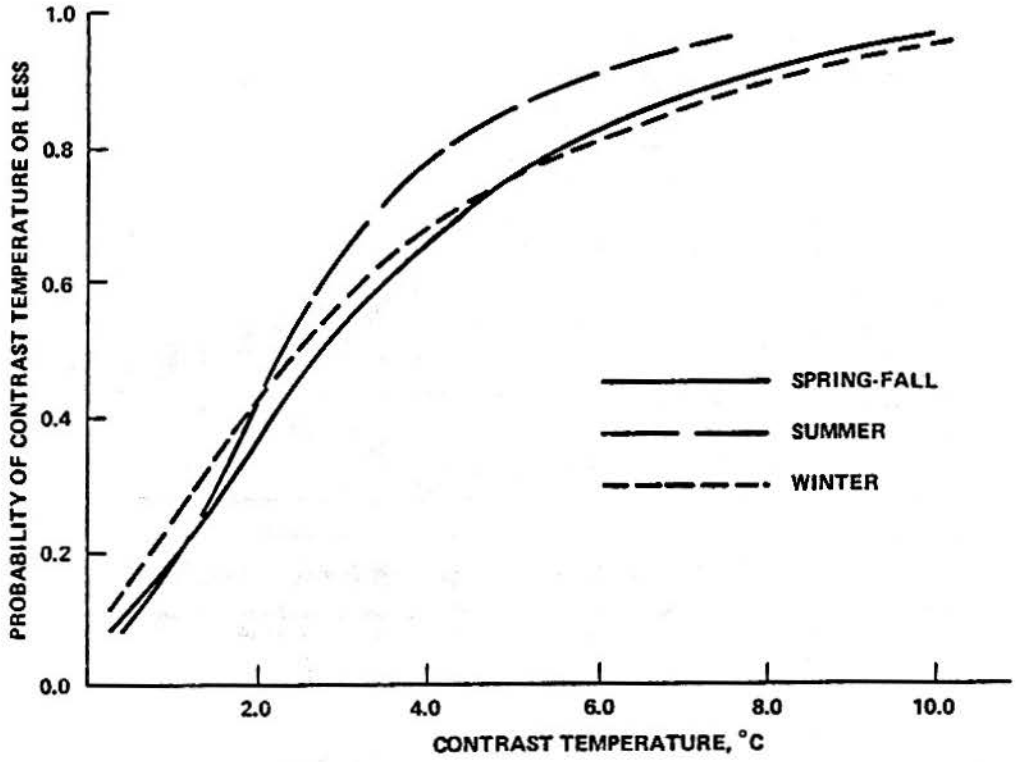

Figure 4. Cumulative probability of observing nighttime contrast temperatures of ships[5]

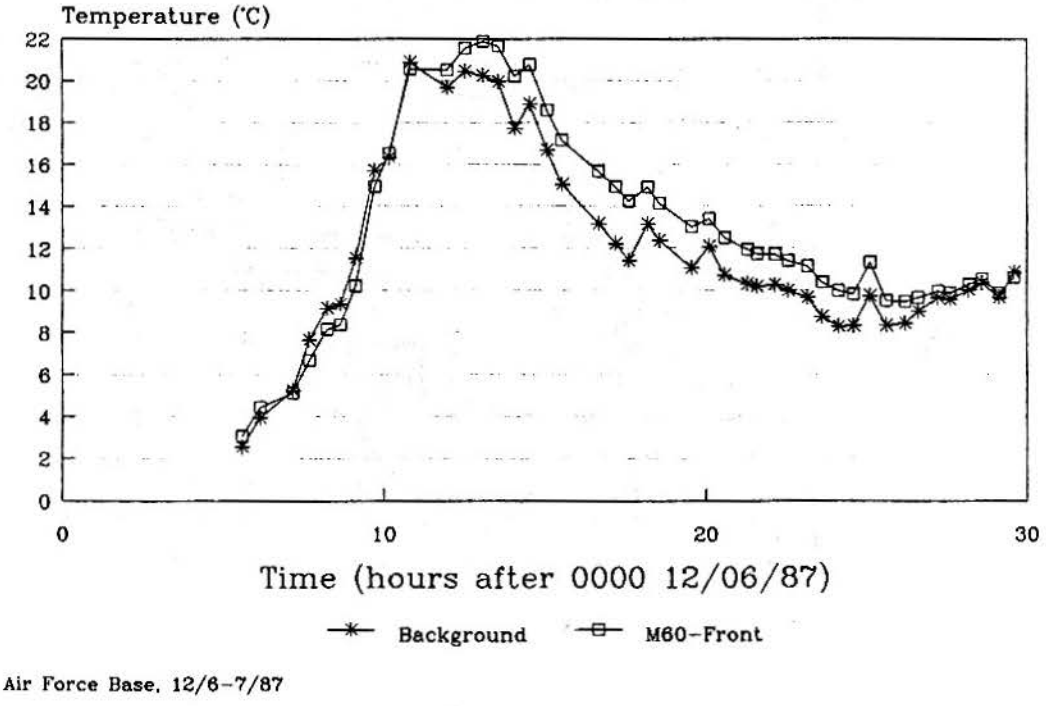

Figure 5. Radiation temperature of the front of a static M60 tank and its grassy background as a function of time

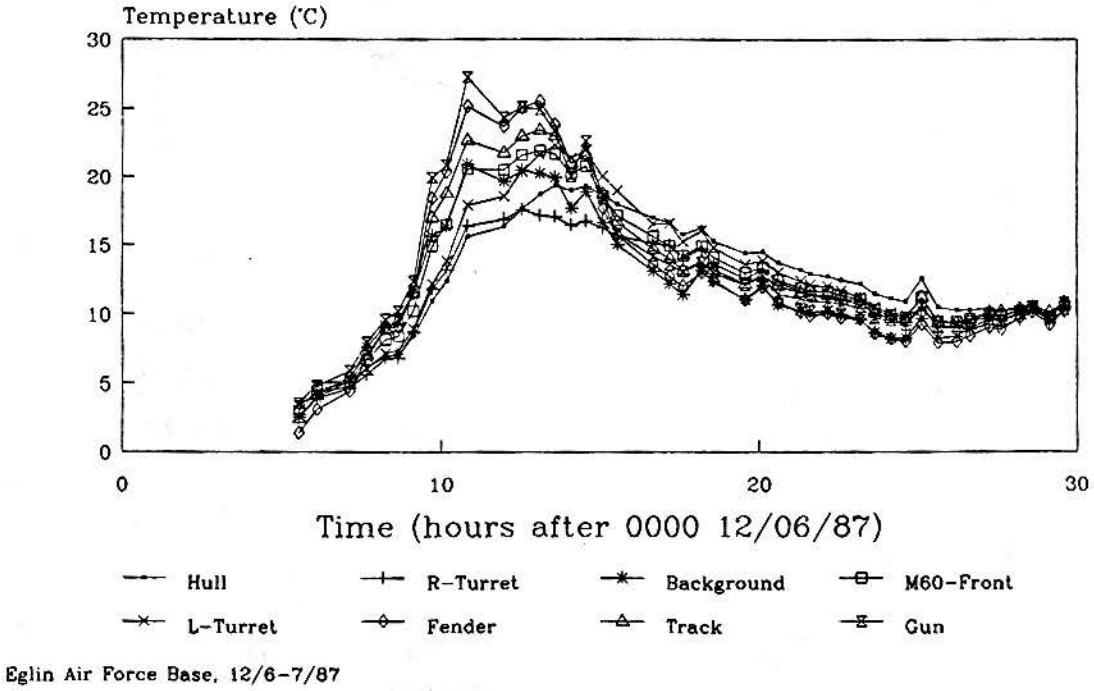

Figure 6. Radiation temperatures of features of the front of a static M60 tank and its grassy background as a function of time

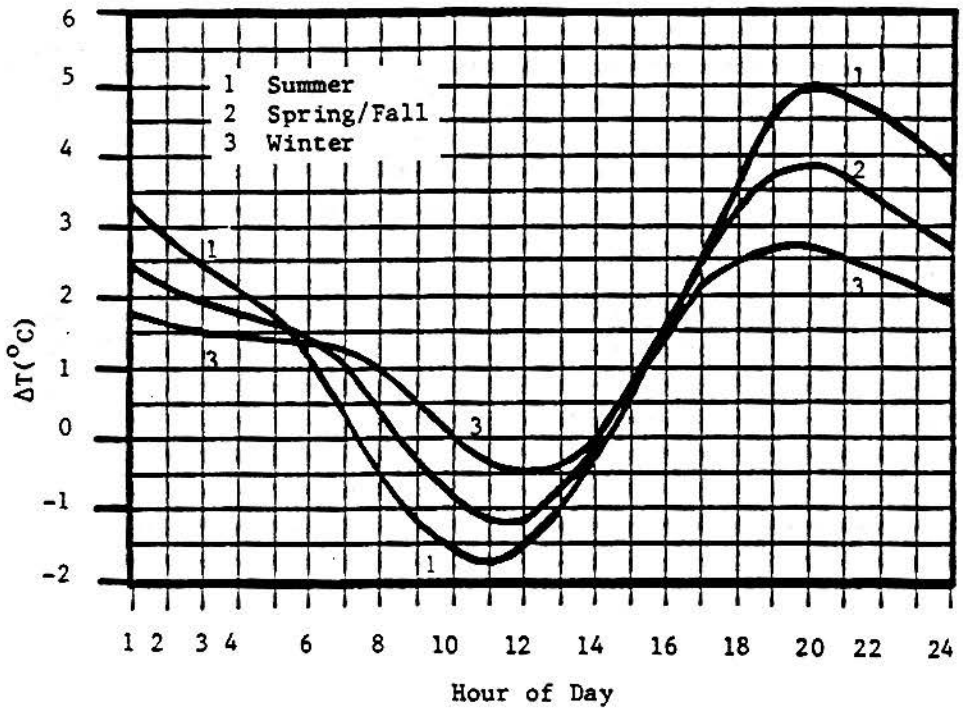

Figure 7. Predicted temperature difference between the front of a tank and its background as a function of time and season for clear weather conditions in central Europe[8]

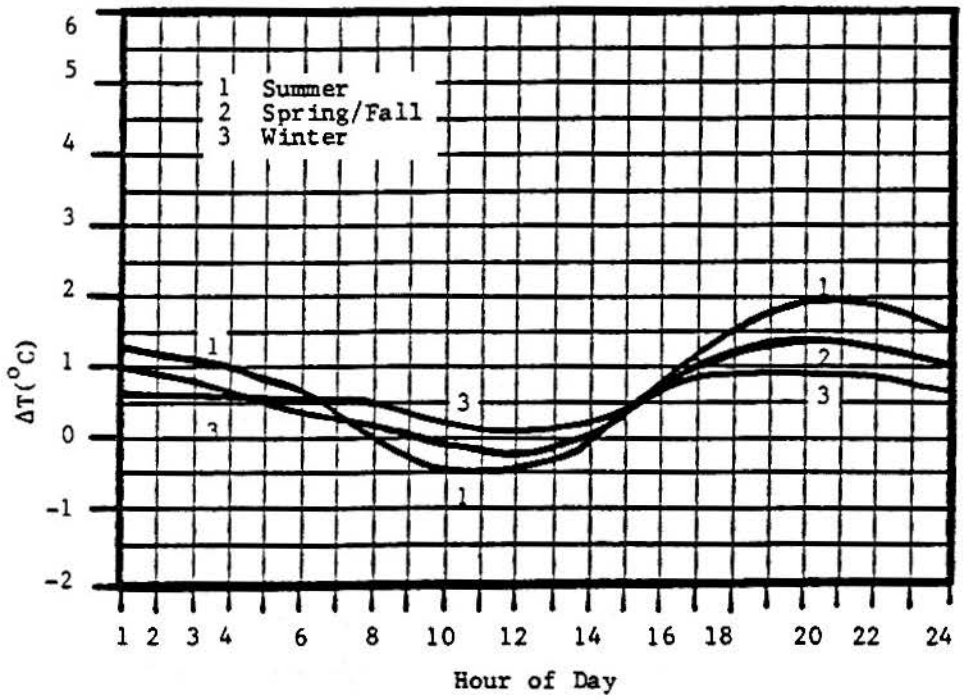

Figure 8. Predicted temperature difference between the front of a tank and its background as a function of time and season for overcast weather conditions in central Europe[8]

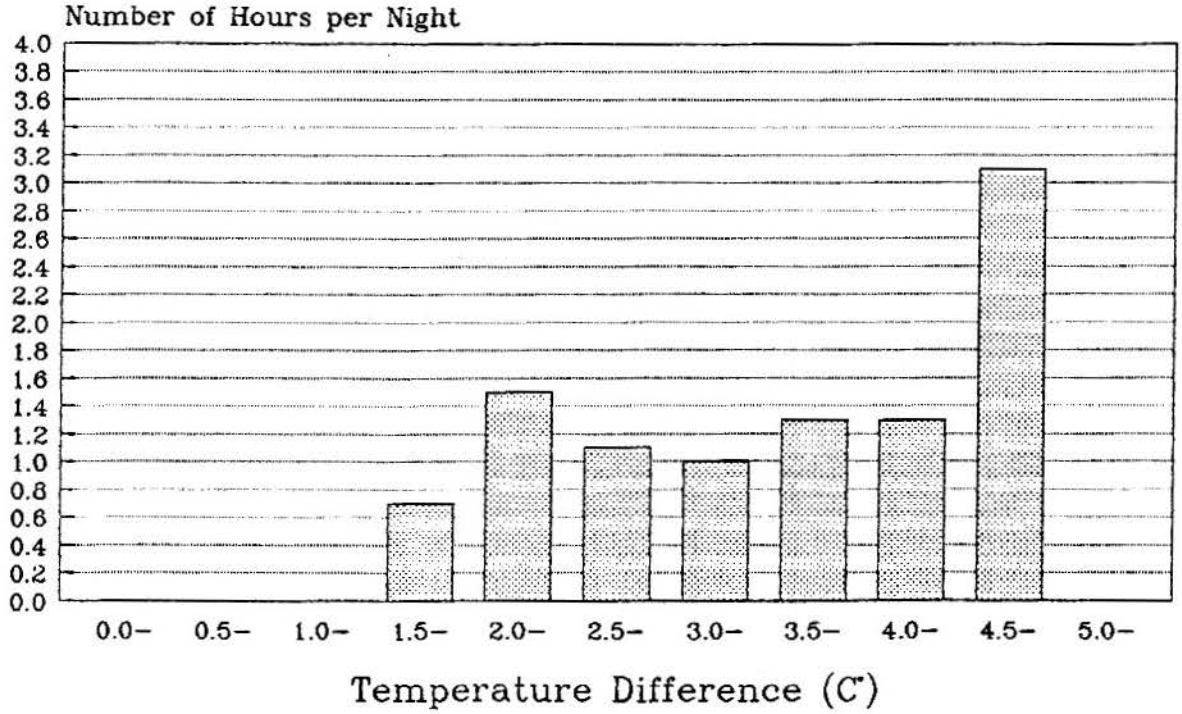

Figure 9. Predicted number of hours per night that the temperature difference between a tank and its background will fall within indicated temperature intervals under clear summertime conditions in central Europe

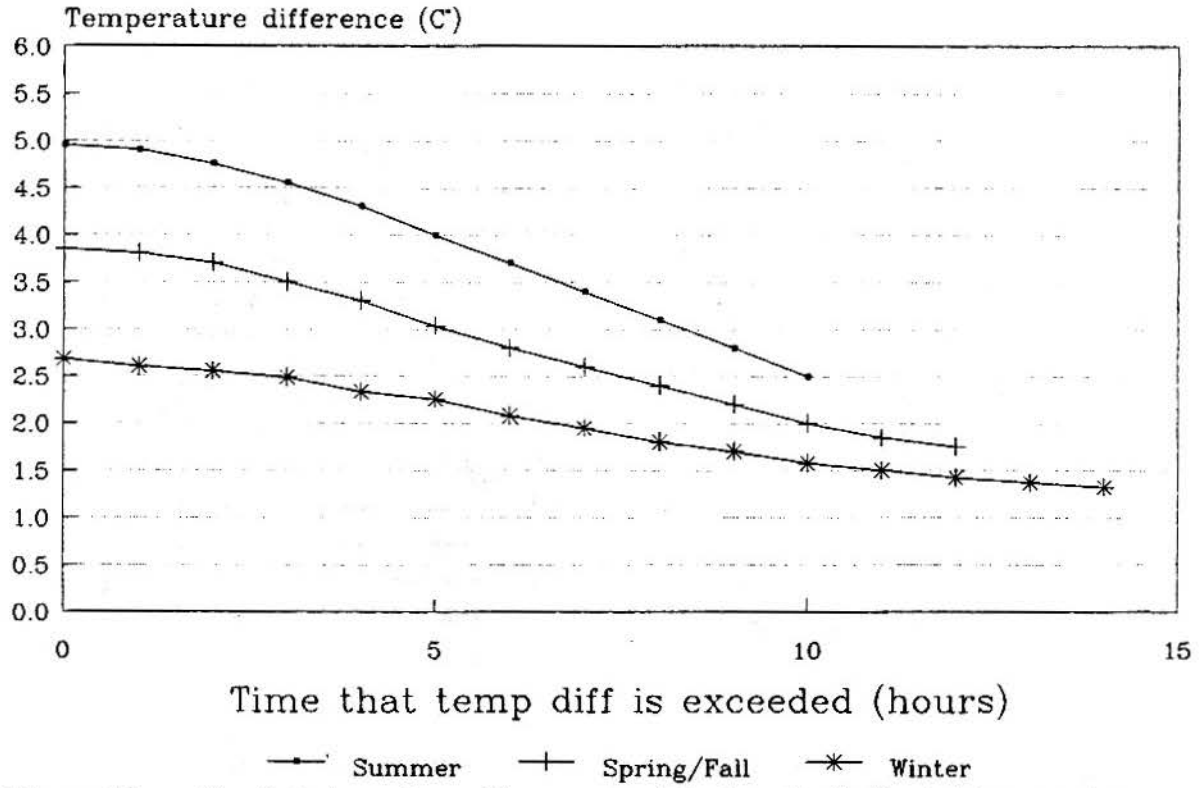

Figure 10. Predicted number of hours per night that the indicated temperature differences between a tank and its background will be exceeded under clear conditions in central Europe

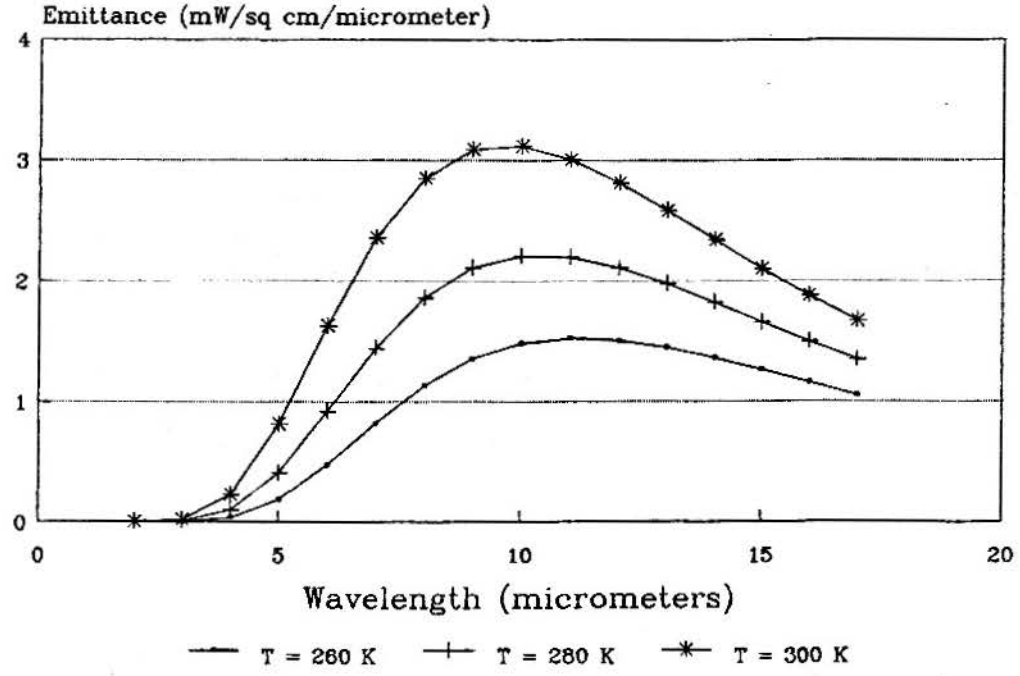

Figure 11. Spectral radiant emittance of a blackbody over the 2- to 17-μm band for three temperatures

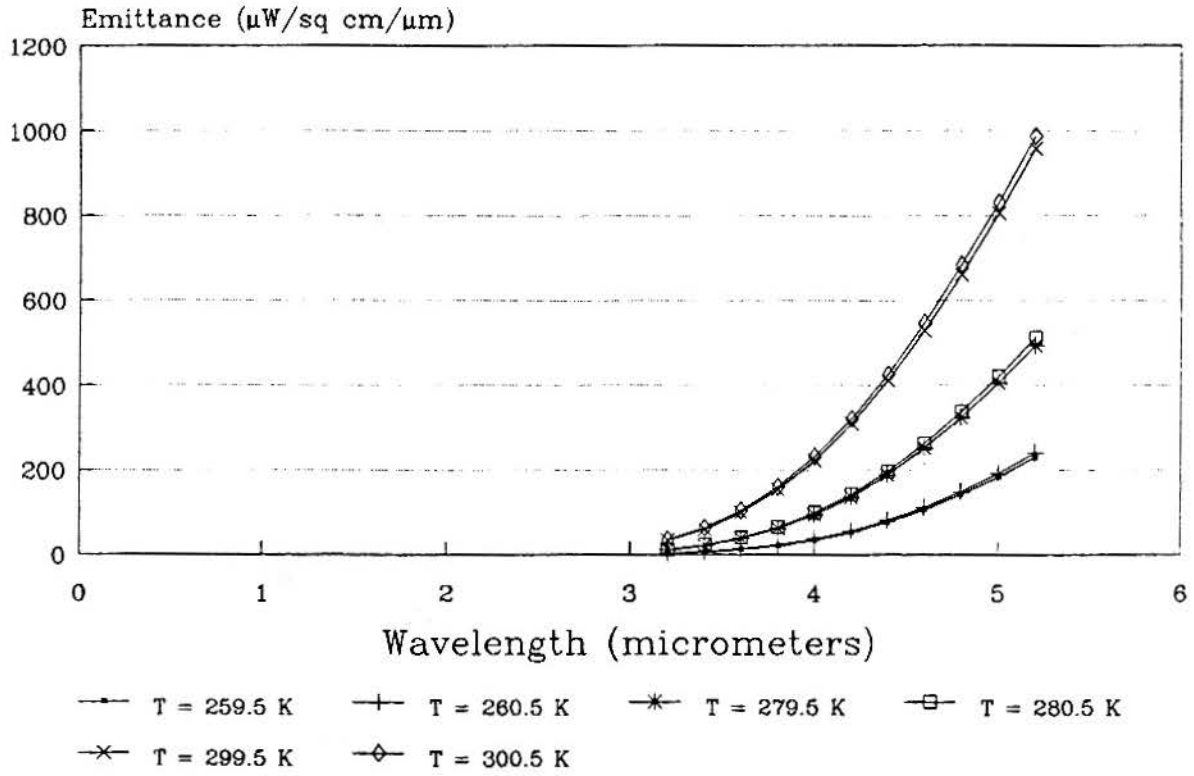

Figure 12. Spectral radiant emittance of a blackbody over the 3.2- to 5.2-μm for six temperatures

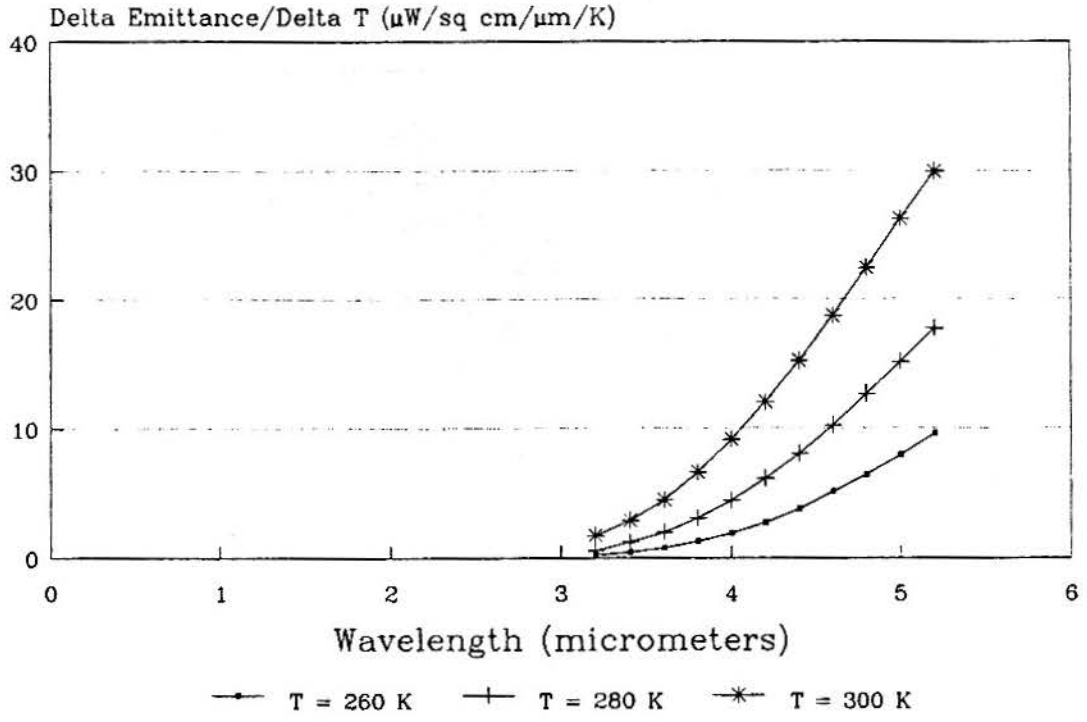

Figure 13. Incremental change in spectral radiant emittance of a blackbody per kelvin change in temperature over the 3.2- to 5.2-μm band for three temperatures

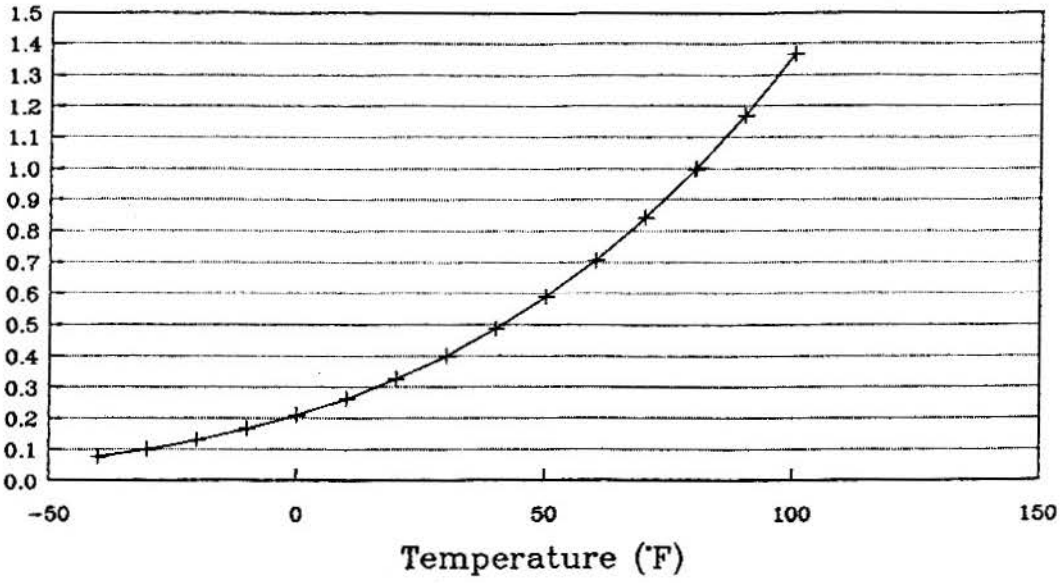

3.4- to 5.0-μm band

Figure 14. Relative signal in the 3.4- to 5.0-μm band as a function of scene temperature referenced to a 300-K background

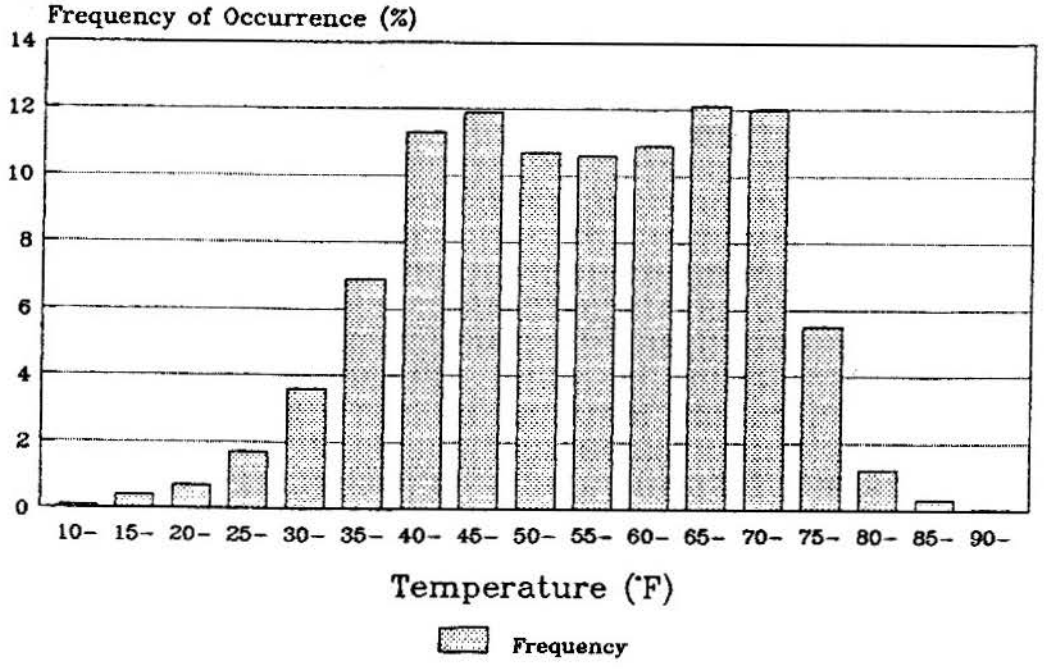

Annual, 40N-Coast, 72W-Coast, day/night

Figure 15. Frequency of occurrence of air temperatures within 5-F° intervals for the marine area near New York, NY, day and night, on an annual basis

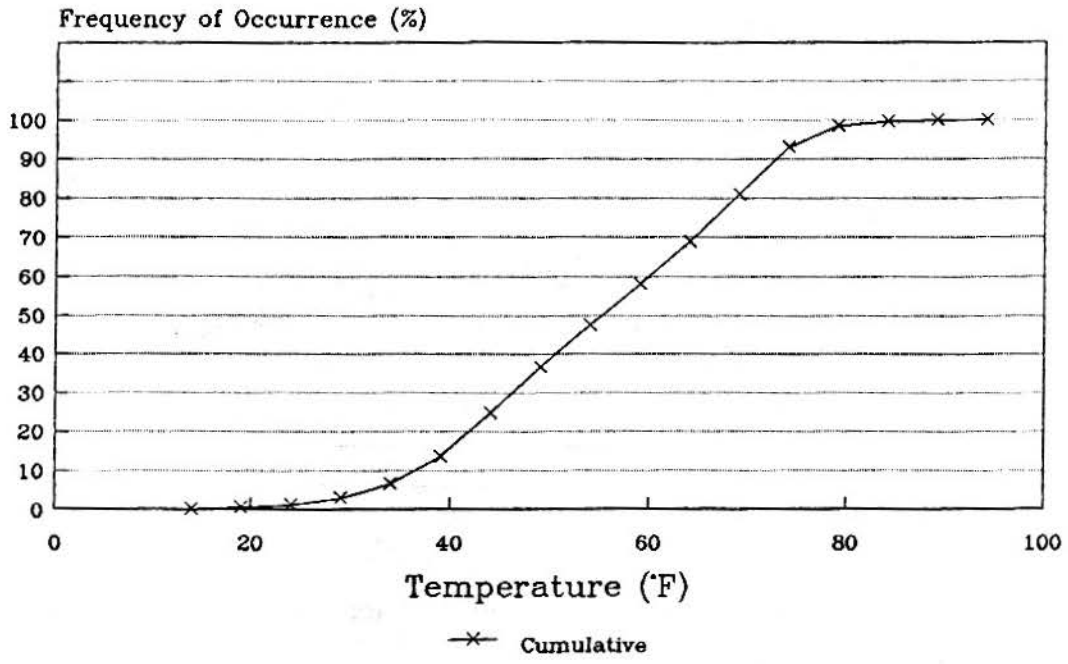

40N-Coast, 72W-Coast; annual; day/night

Figure 16. Cumulative frequency of occurrence of indicated air temperatures for the marine area near New York, NY, day and night, on an annual basis

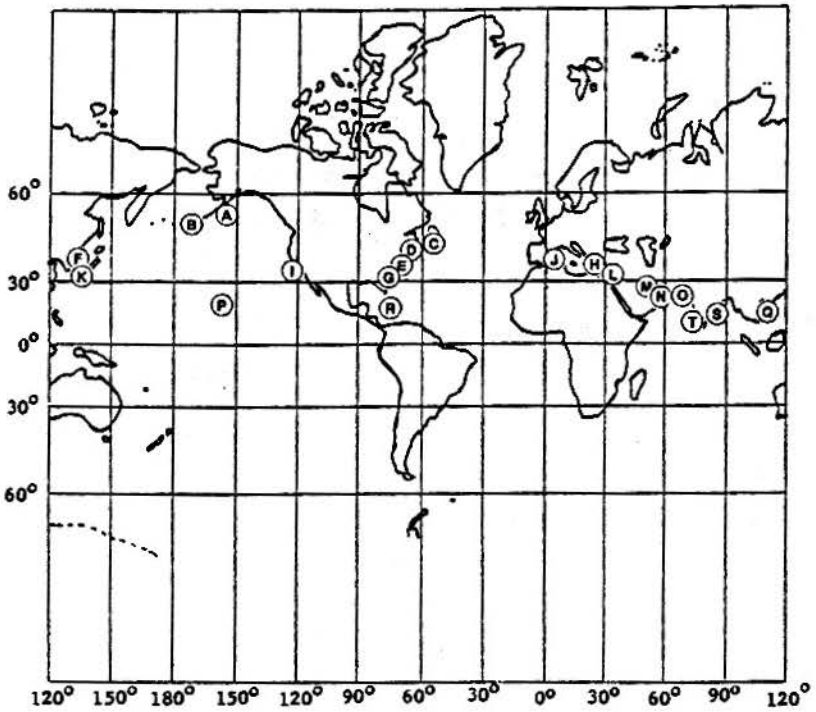

Figure 17. Map of the world indicating the locations of twenty sites (listed in table 1) for which temperature data are presented (in figures 18 through 37)

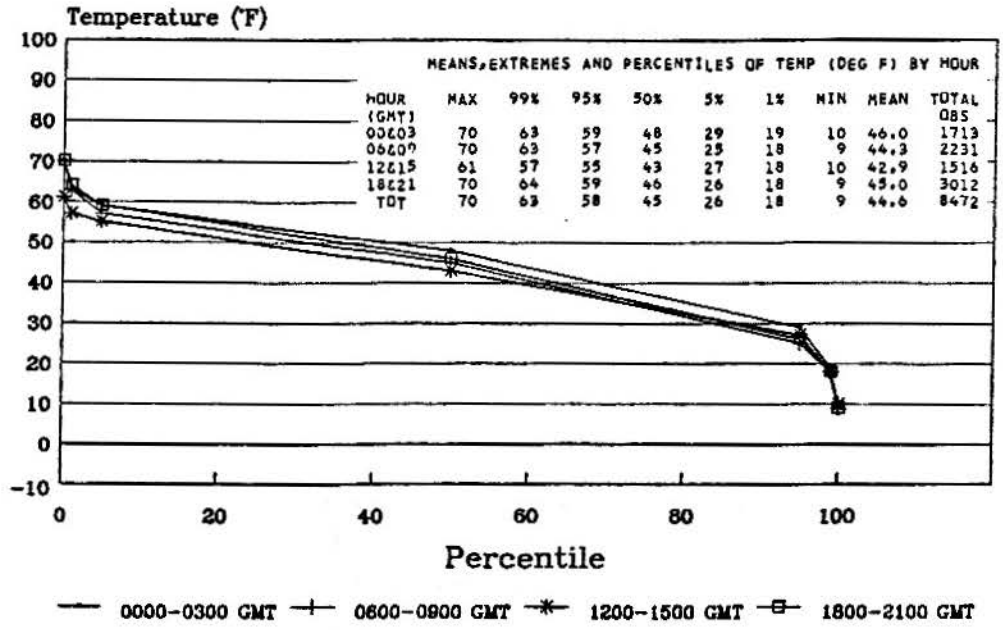

Figure 18. Percentiles of air temperature for the marine area near Kodiak, Alaska

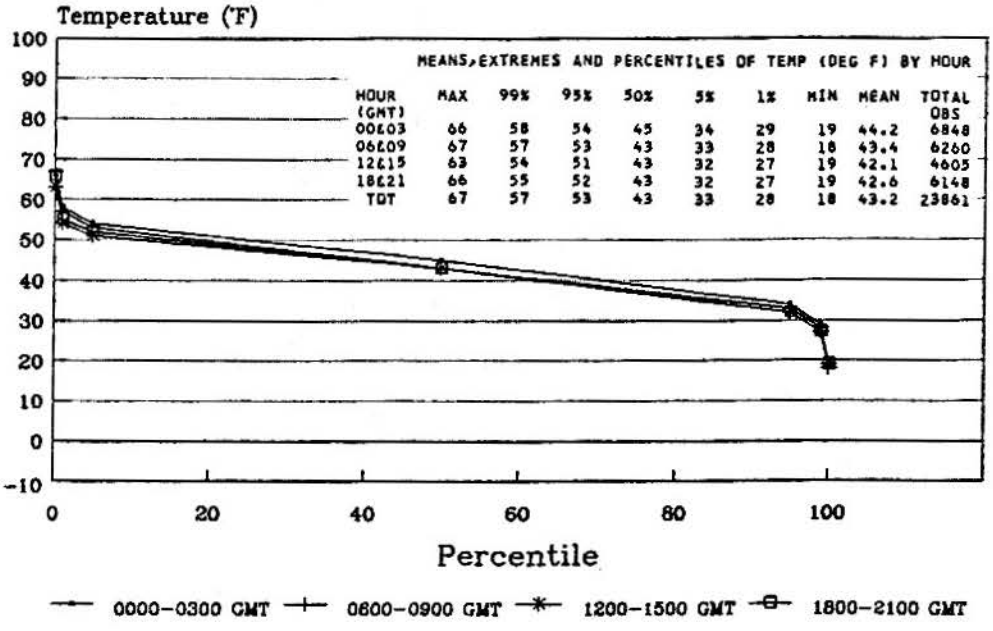

Figure 19. Percentiles of air temperature for the marine area near Adak, Alaska

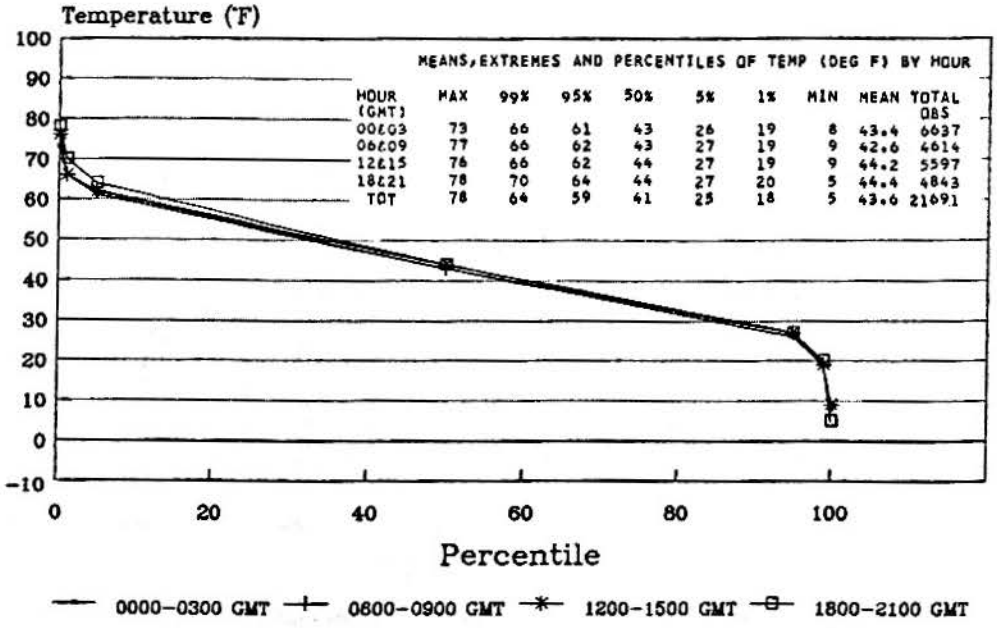

Figure 20. Percentiles of air temperature for the marine area near Argentia, Newfoundland

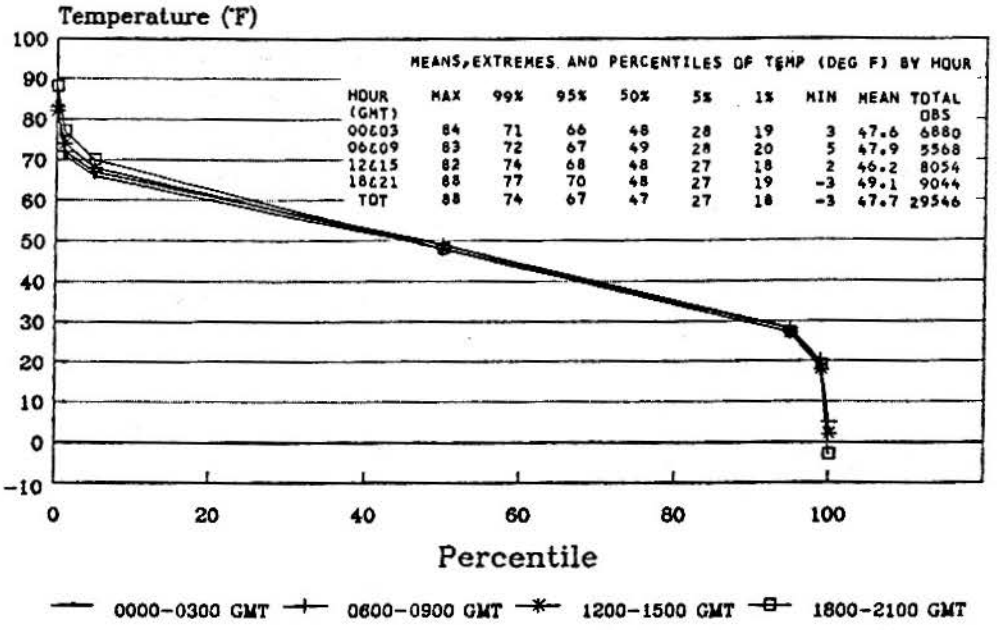

Figure 21. Percentiles of air temperature for the marine area near Boston, Massachusetts

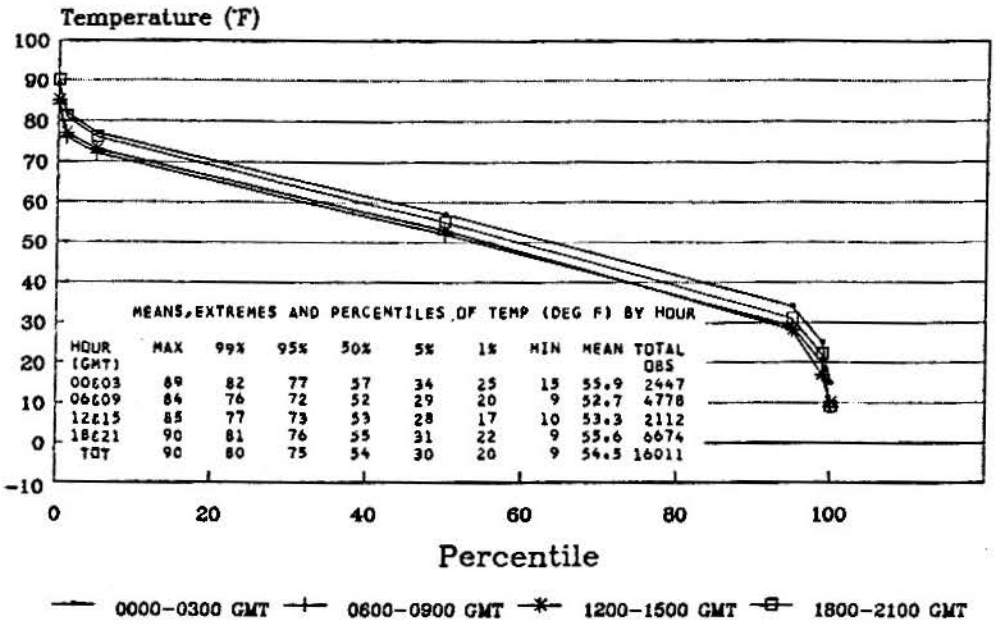

Area: 40N-Coast, 72W-Coast

Figure 22. Percentiles of air temperature for the marine area near New York, New York

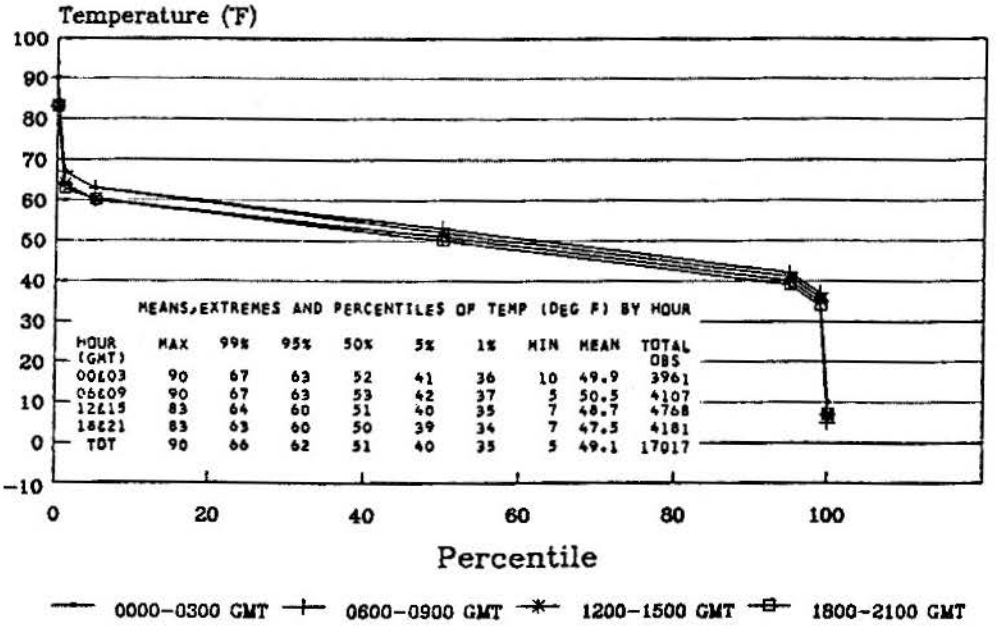

Area: 39.7N, 129.4E

Figure 23. Percentiles of air temperature for the marine area near Wonsan, North Korea

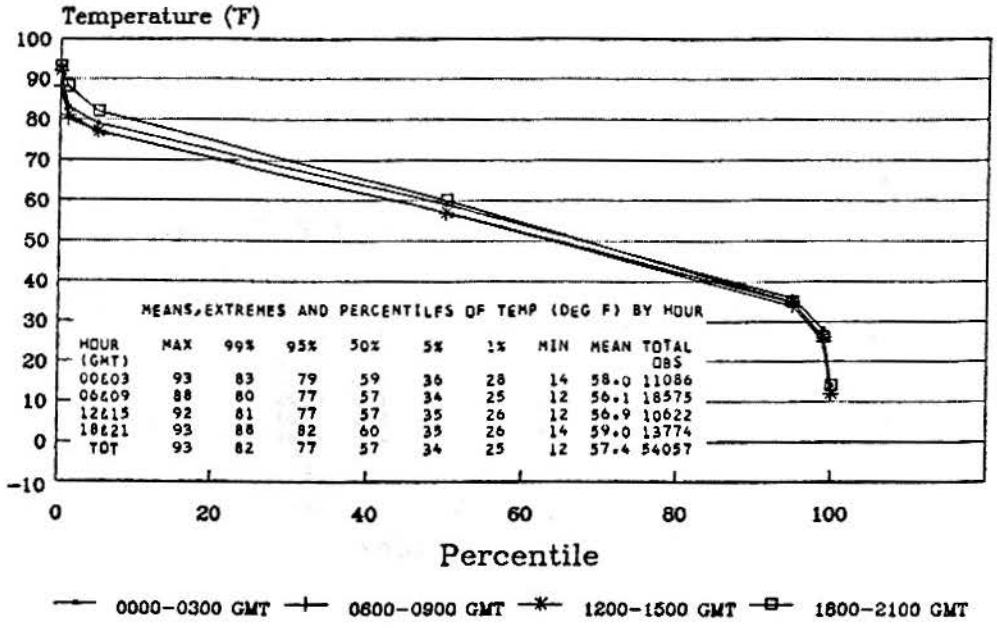

Figure 24. Percentiles of air temperature for the marine area near Atlantic City, New Jersey

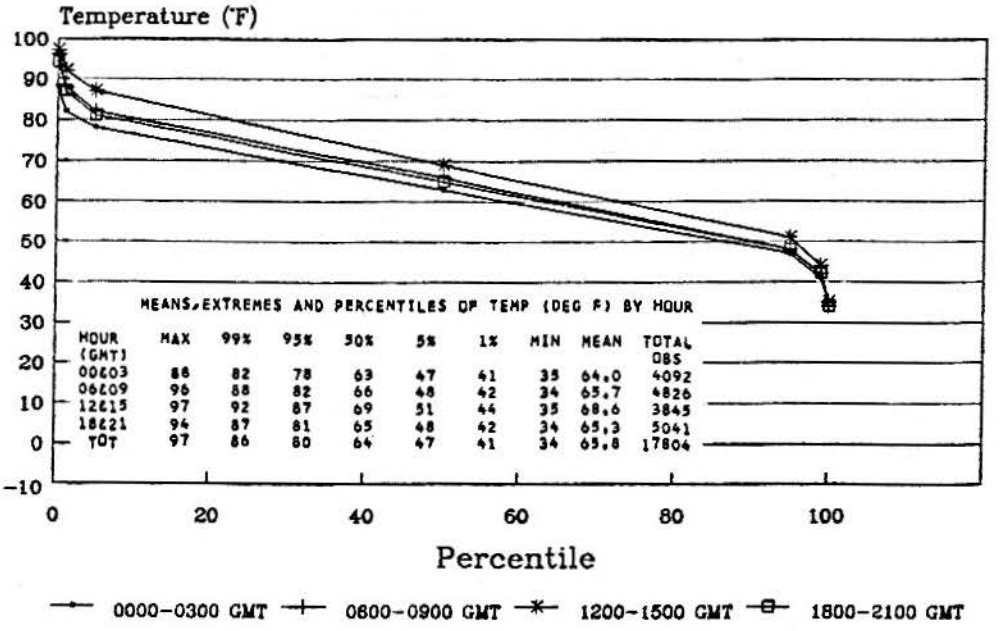

Figure 25. Percentiles of air temperature for the South Aegean Sea

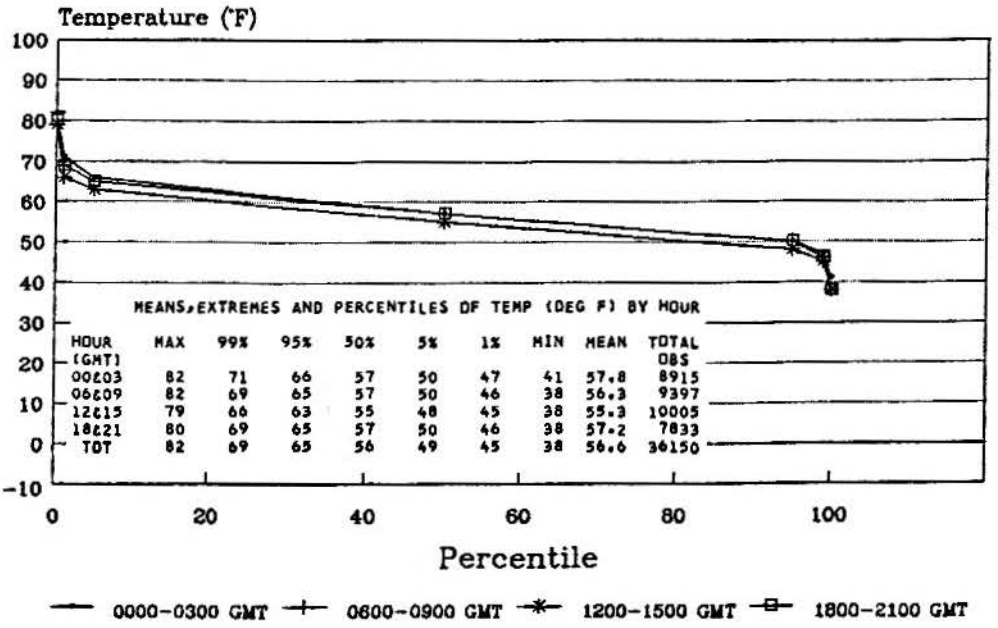

Area: 36-38N, Coast-126W

Figure 26. Percentiles of air temperature for the marine area near San Francisco, California

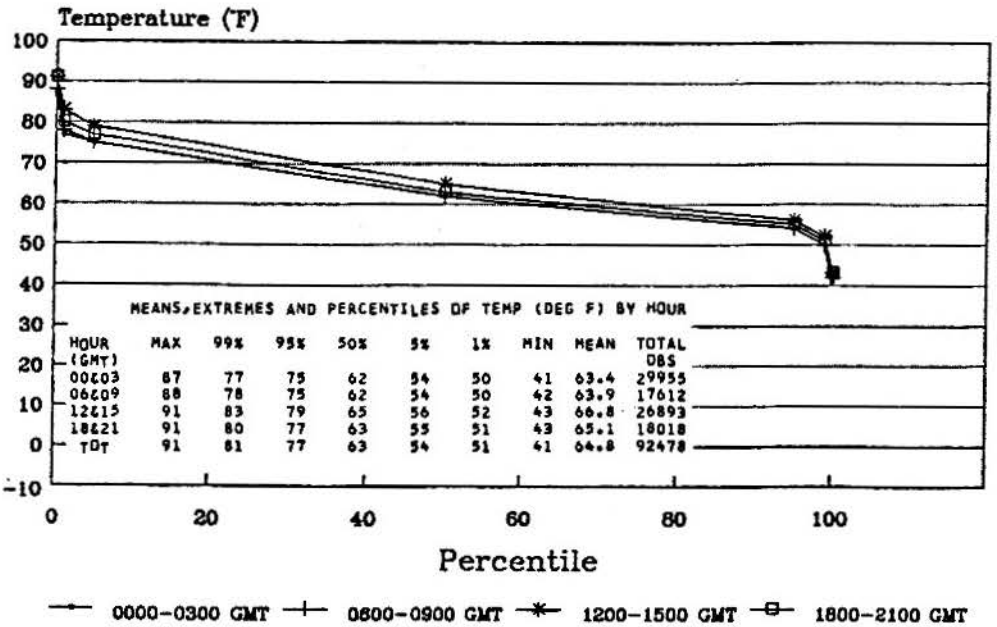

Area: 36.0N, 3.4E

Figure 27. Percentiles of air temperature for the marine area near Malaga, Spain

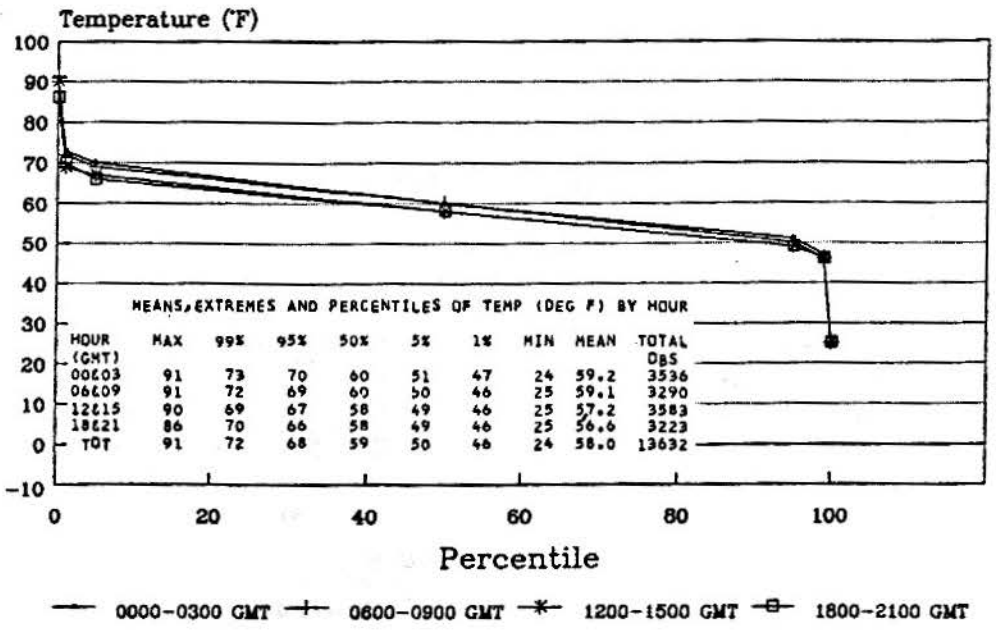

Area: 36.0N, 133.2E

Figure 28. Percentiles of air temperature for the marine area near Matsue, Japan

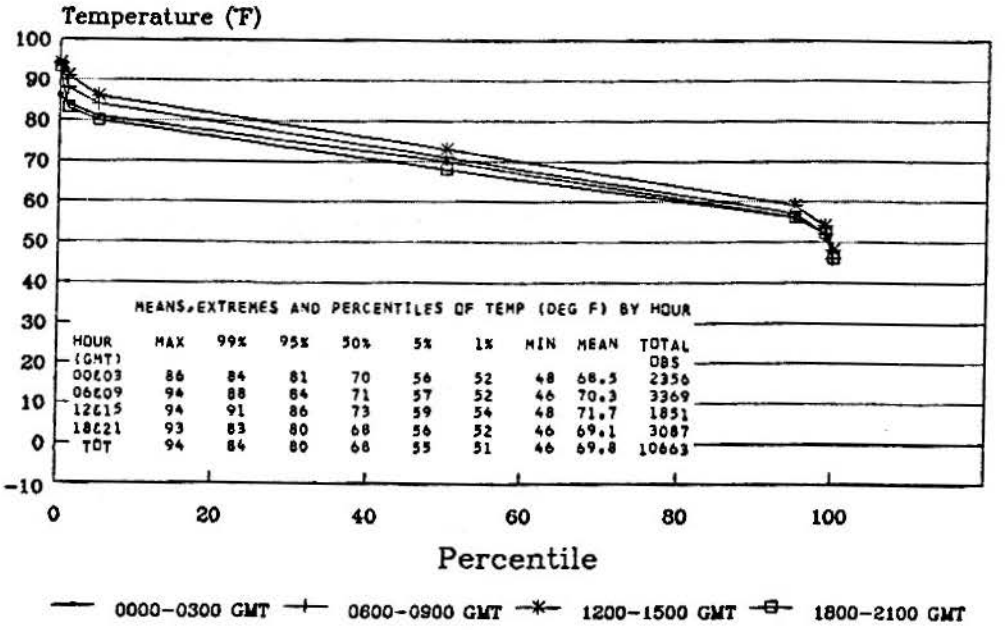

Area: 32.2N, 33.3E

Figure 29. Percentiles of air temperature for the marine area near Port Said, Egypt

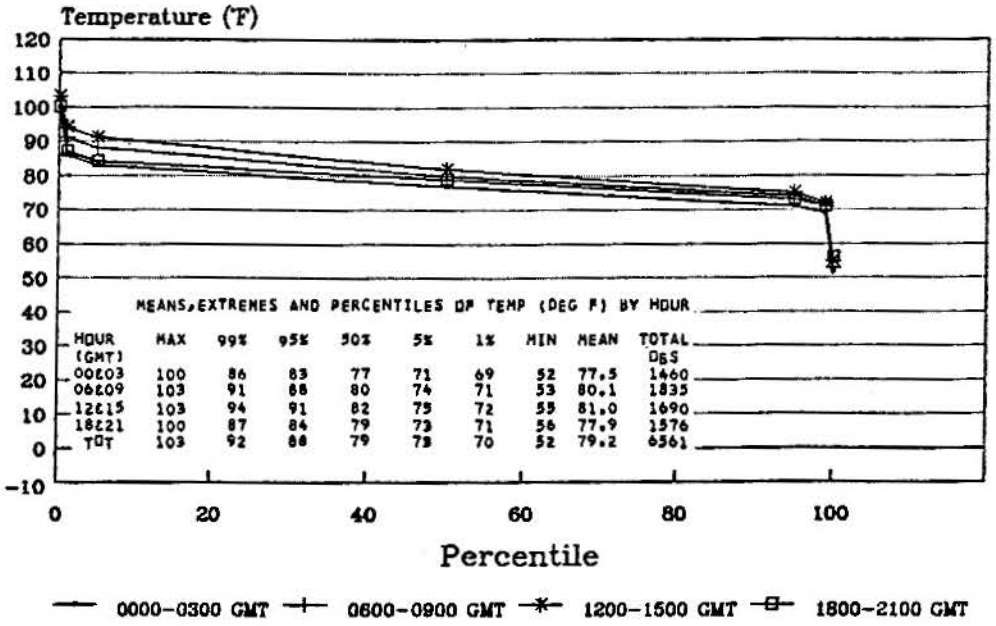

Area: 27.2N, 50.2E

Figure 30. Percentiles of air temperature for the North West Persian Gulf

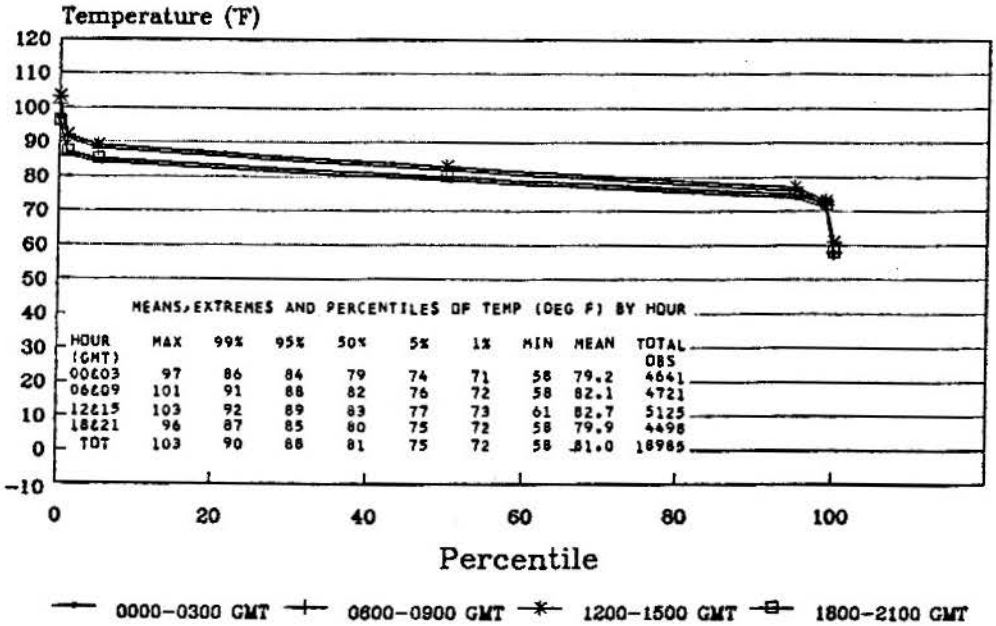

Area: 25.0N, 57.8E

Figure 31. Percentiles of air temperature for the North Gulf of Oman

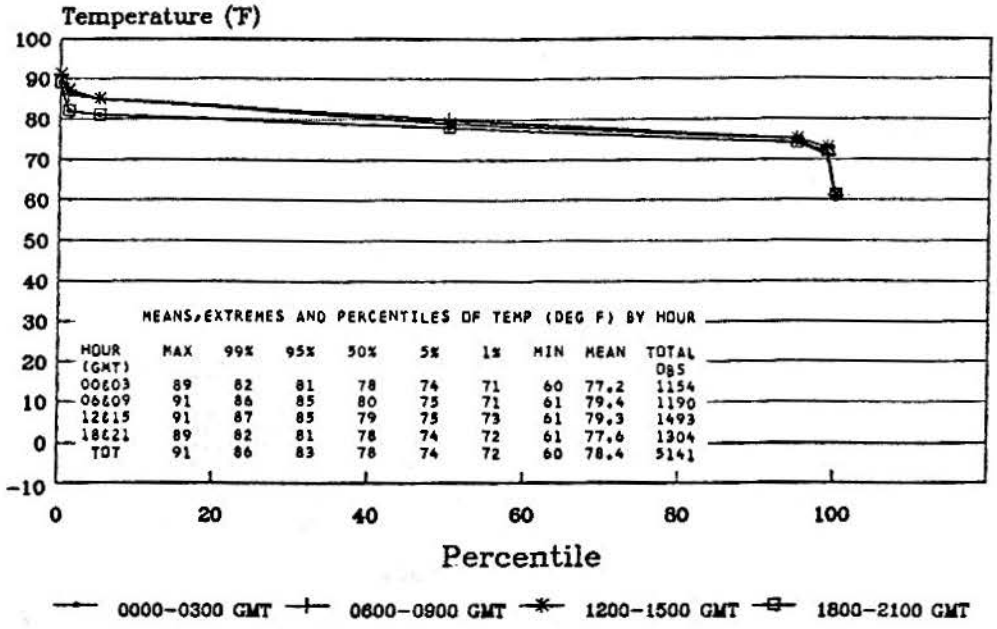

Area: 22.9N, 67.8E

Figure 32. Percentiles of air temperature for the marine area near Karachi, Pakistan

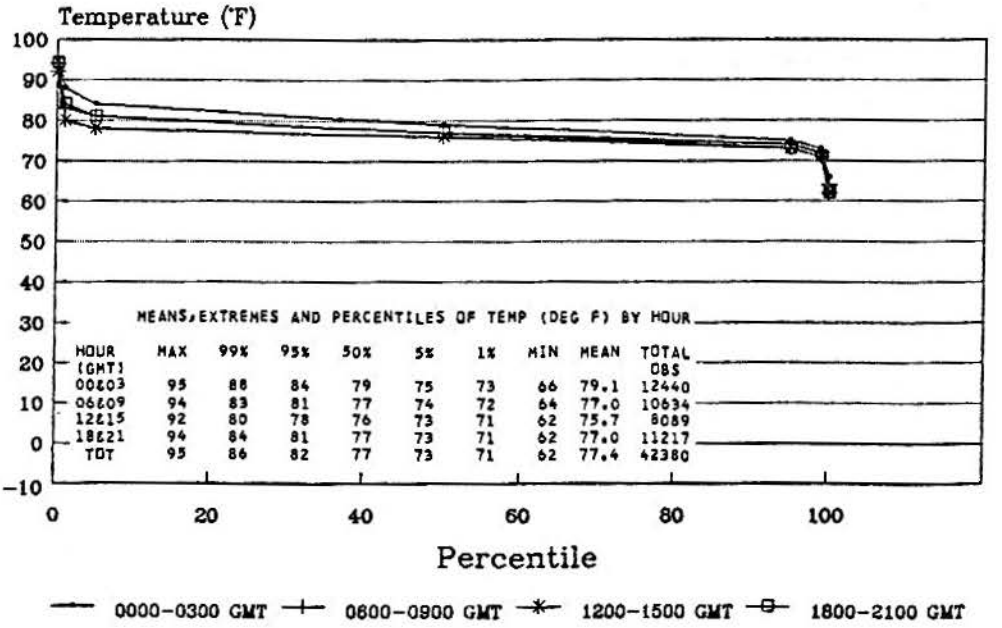

Area: 20.4N, 158.3W

Figure 33. Percentiles of air temperature for the Hawaiian Leeward

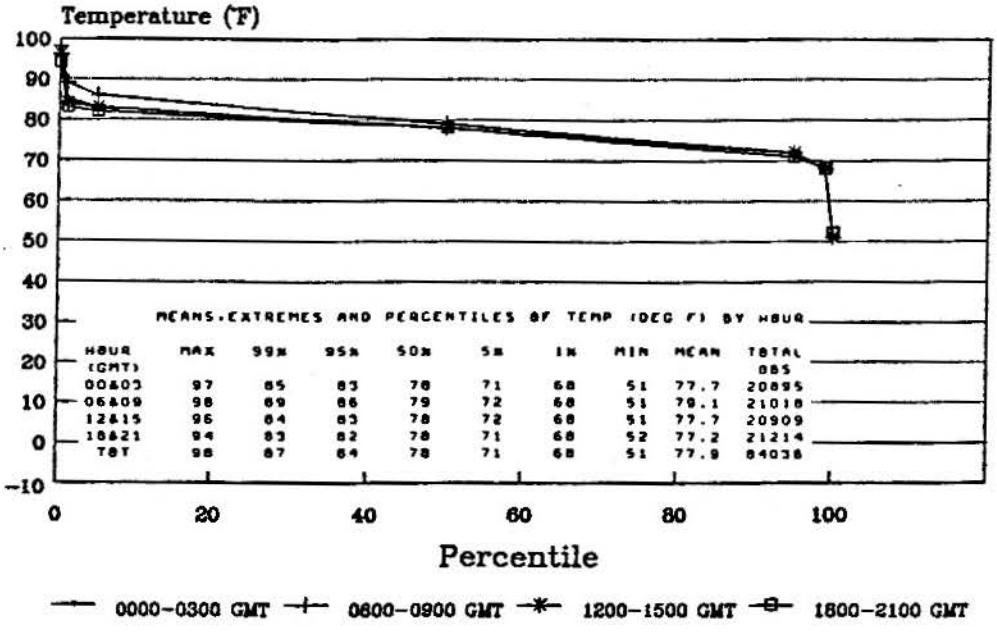

Area: 18.3N, 107.5E

Figure 34. Percentiles of air temperature for the Tonkin Gulf

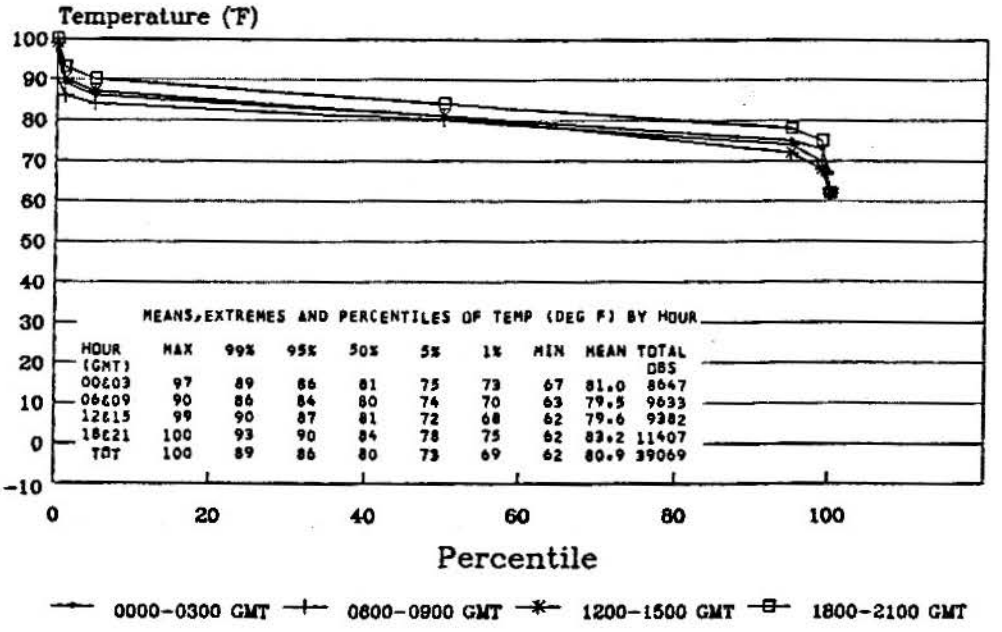

Area: 18-20N, 74-76W

Figure 35. Percentiles of air temperature for the marine area near Guantanamo, Cuba

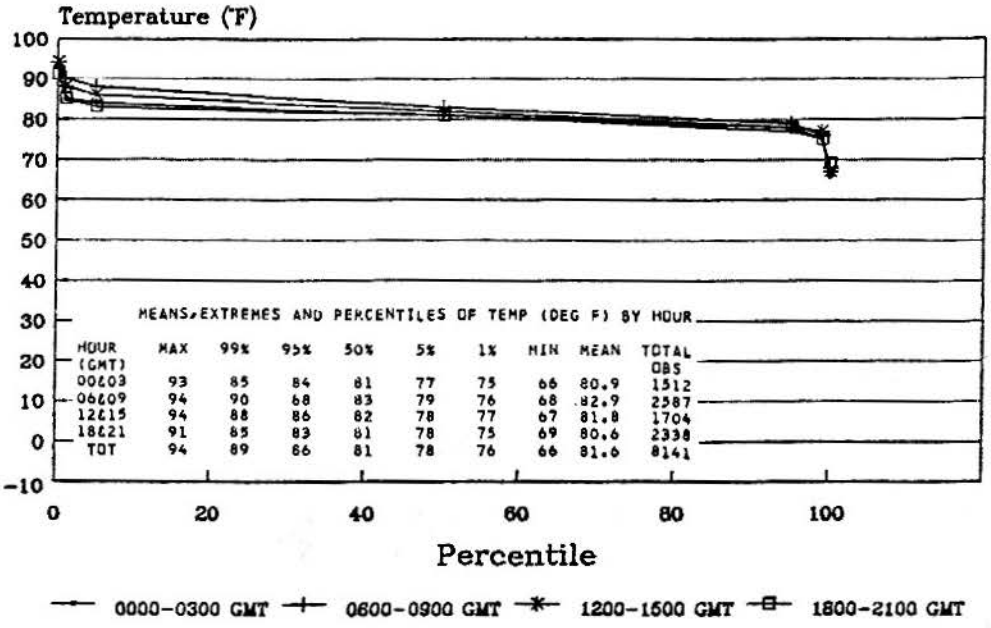

Area: 17.9N, 85.2E

Figure 36. Percentiles of air temperature for the marine area near Vishakhapatnam, India

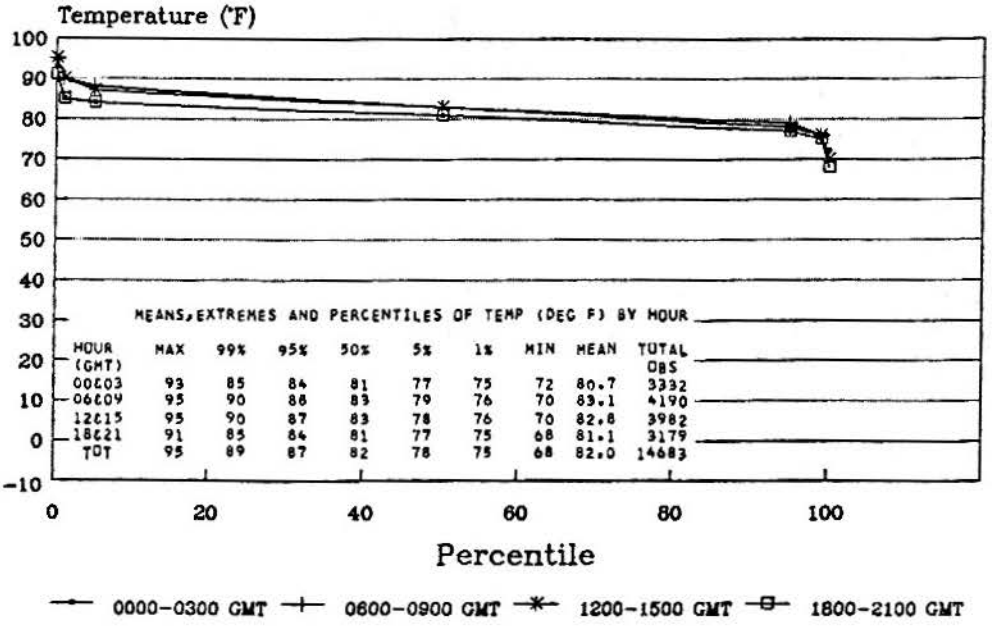

Area: 14.2N, 73.0E

Figure 37. Percentiles of air temperature for the marine area near Panjim, Goa

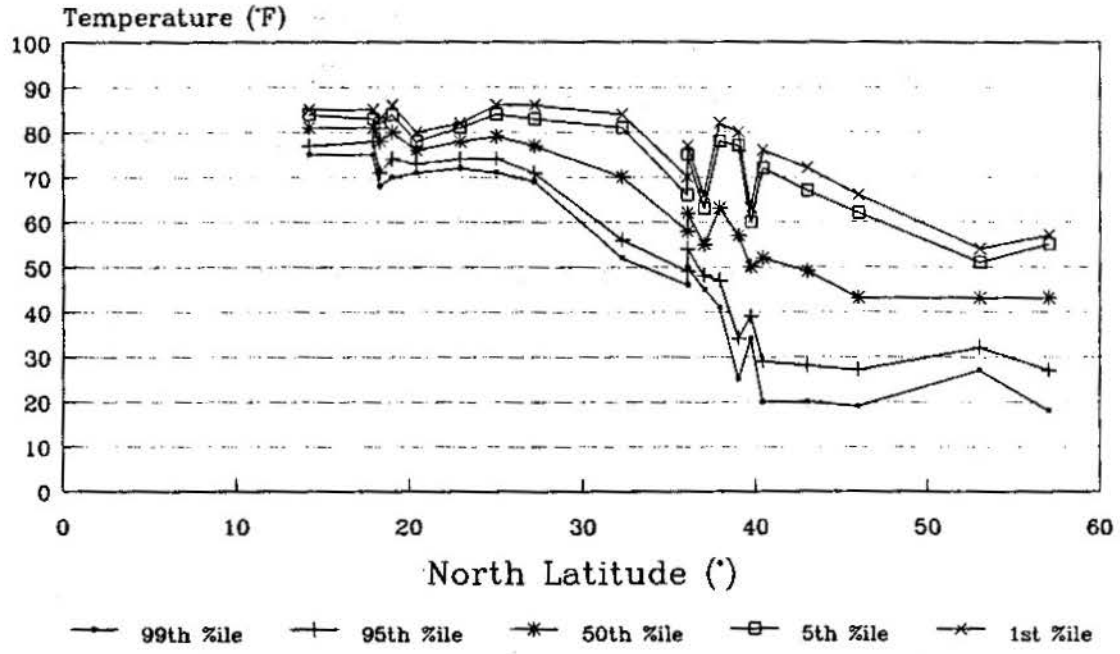

Twenty selected marine areas, annual

Figure 38. Nighttime air temperature by percentile as a function of latitude of twenty selected maritime sites

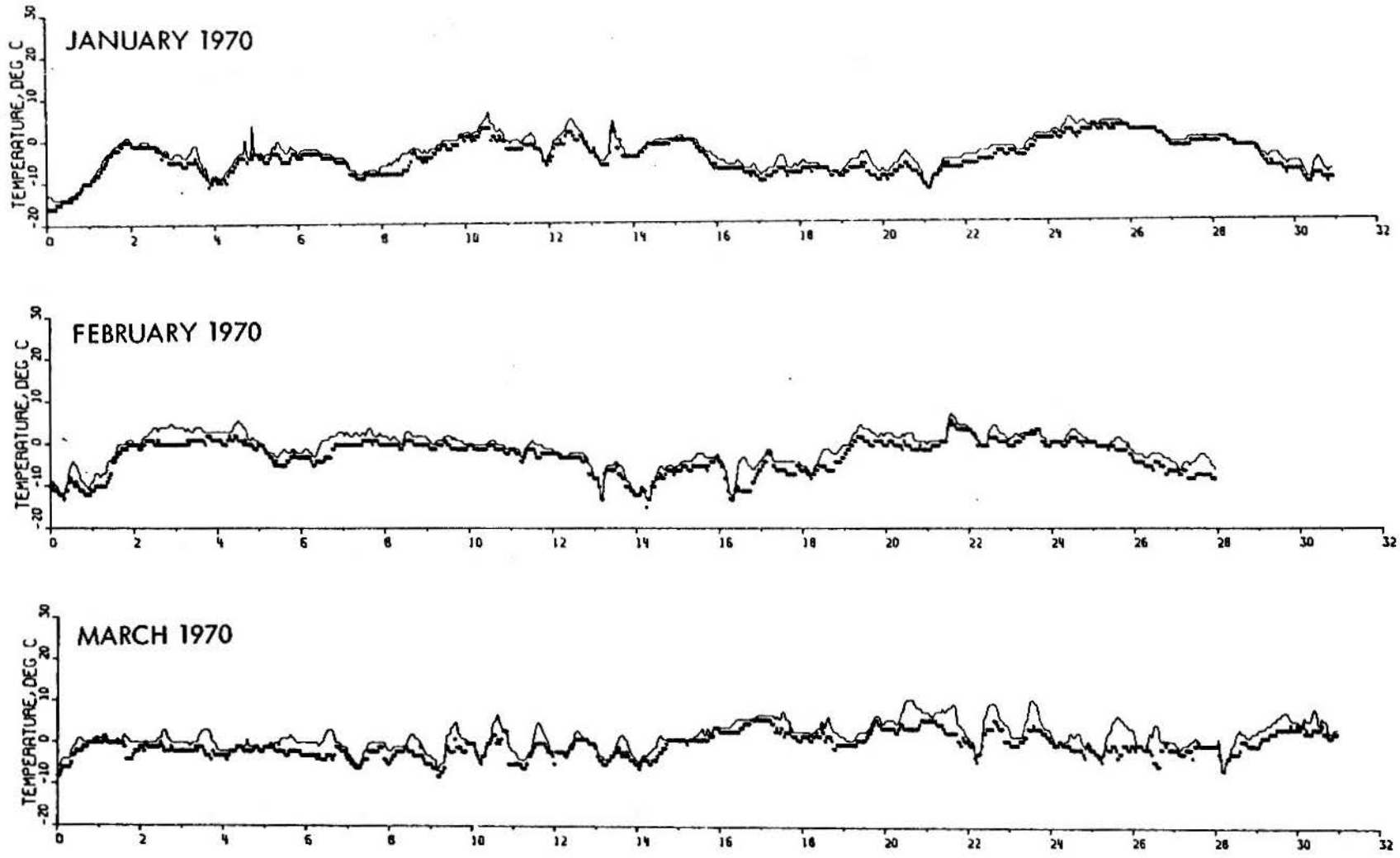

Figure 39. Hourly readings of air temperature and dew point at Hannover, Germany, for January - March 1970

_____ air temperature _____ dew point

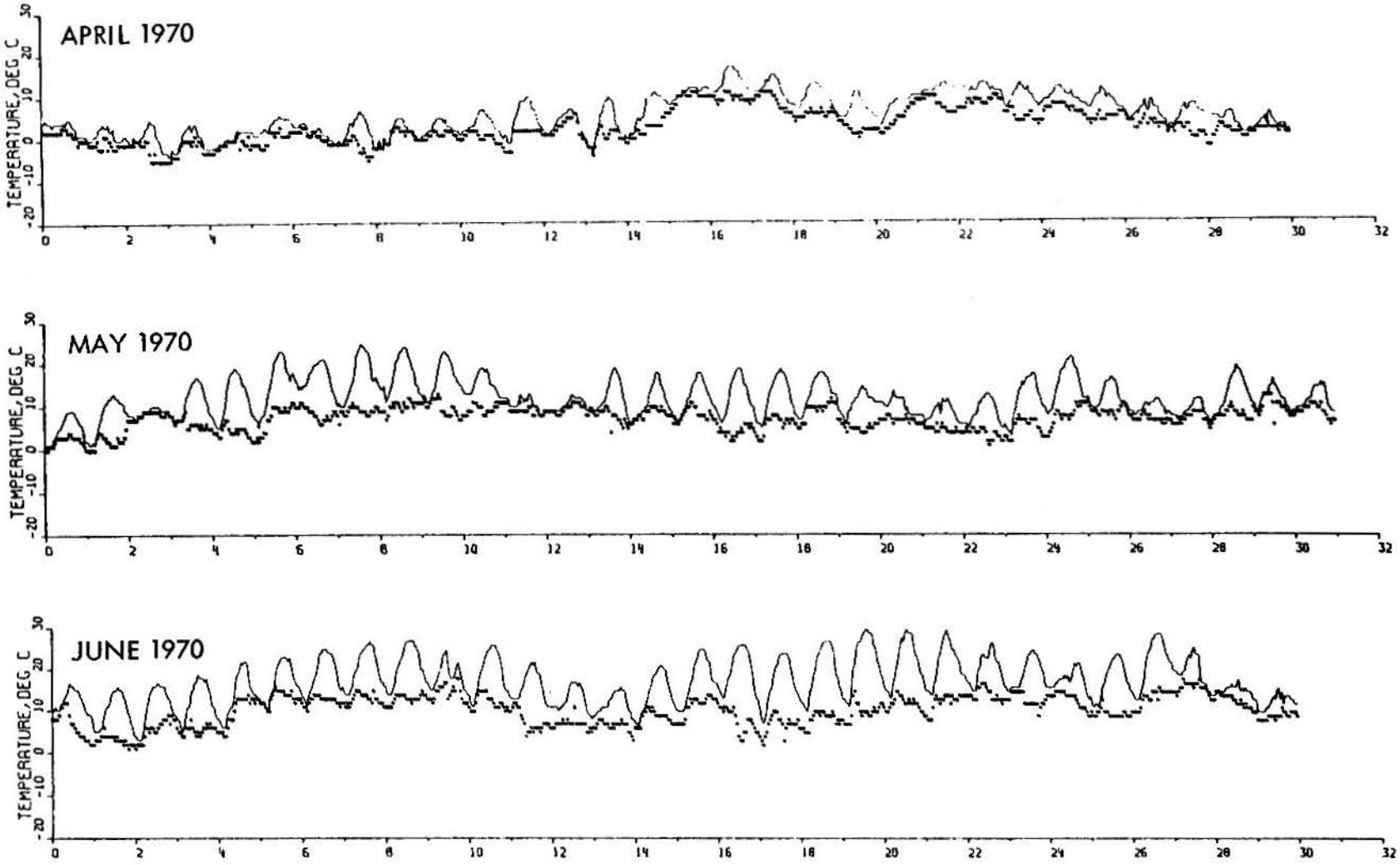

Figure 40. Hourly readings of air temperature and dew point at Hannover, Germany, for April - June 1970

_____ air temperature _____ dew point

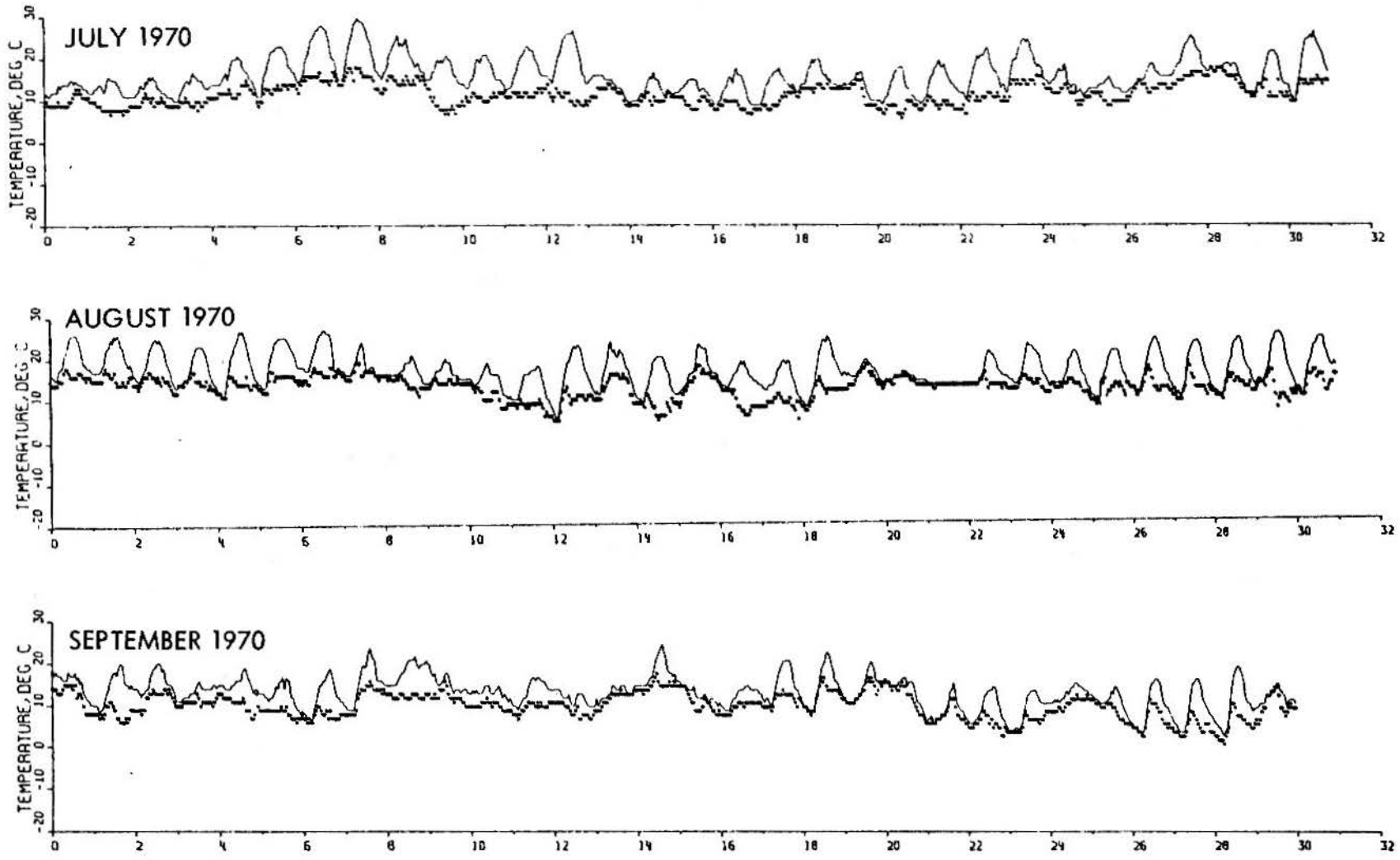

Figure 41. Hourly readings of air temperature and dew point at Hannover, Germany, for July - September 1970

_____ air temperature _____ dew point

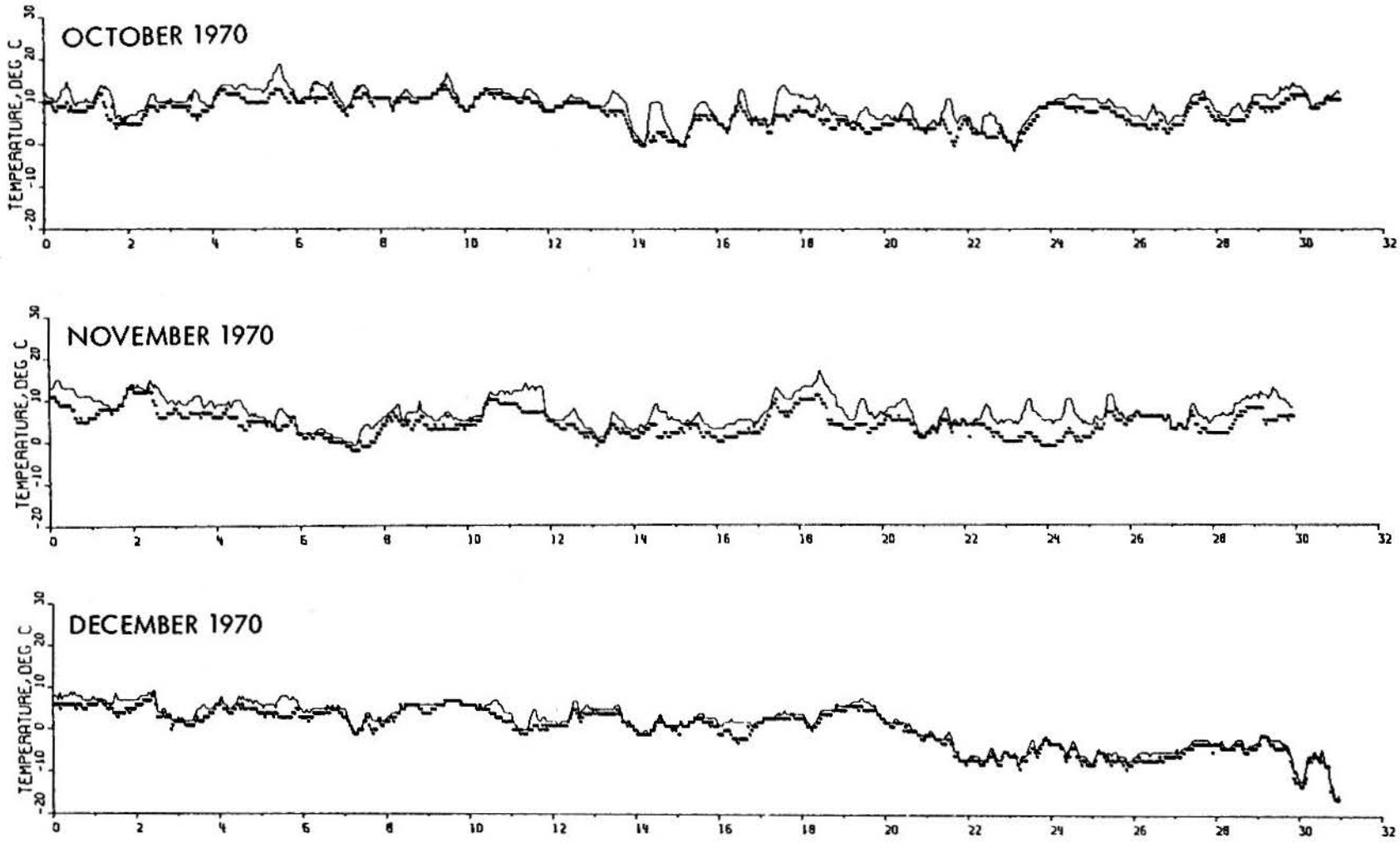

Figure 42. Hourly readings of air temperature and dew point at Hannover, Germany, for October - December 1970

_____ air temperature _____ dew point

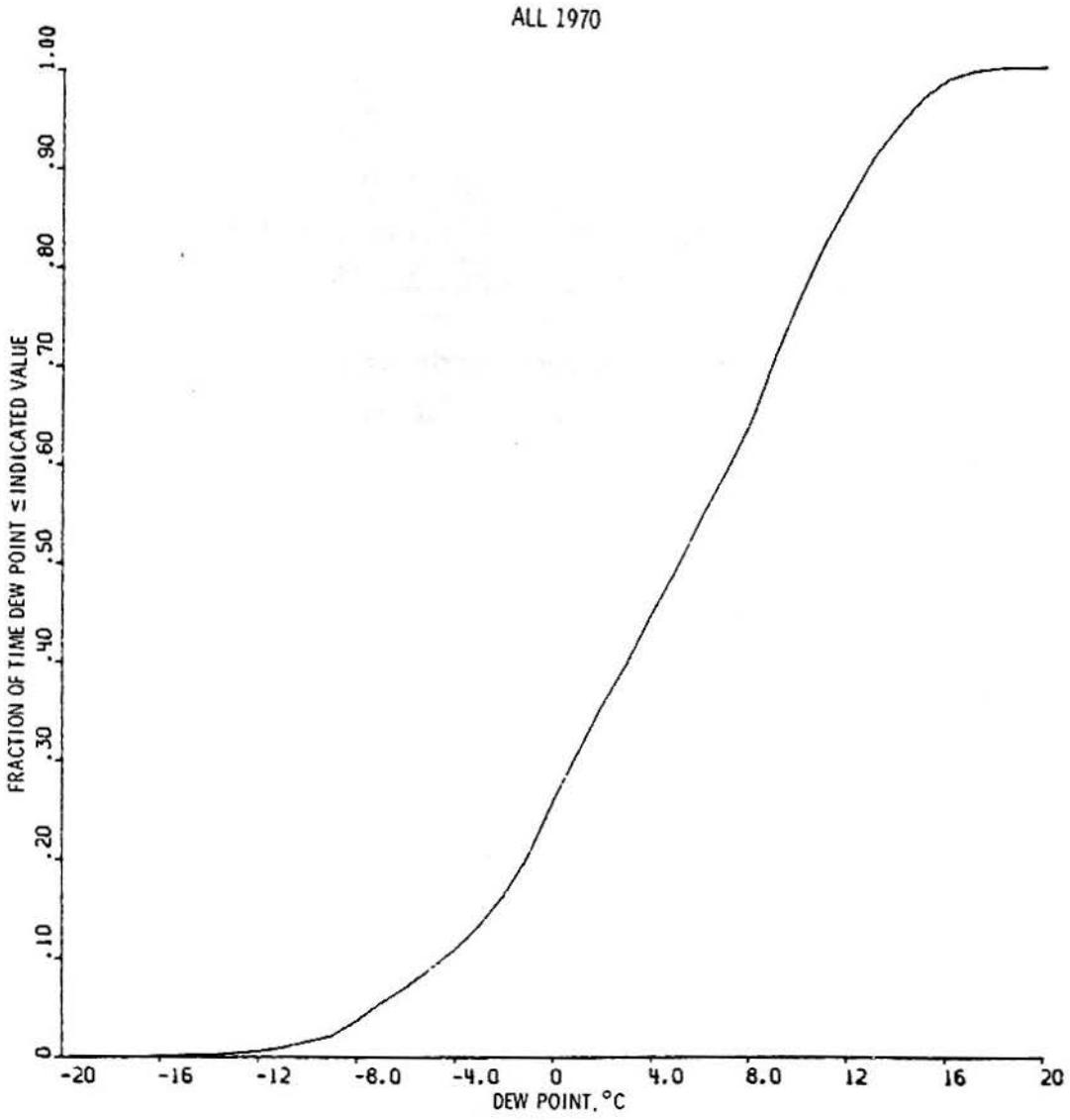

Figure 43. Fractions of the hourly readings for which the dew point at Hannover, Germany, was at or below the indicated temperatures for the year 1970[10]

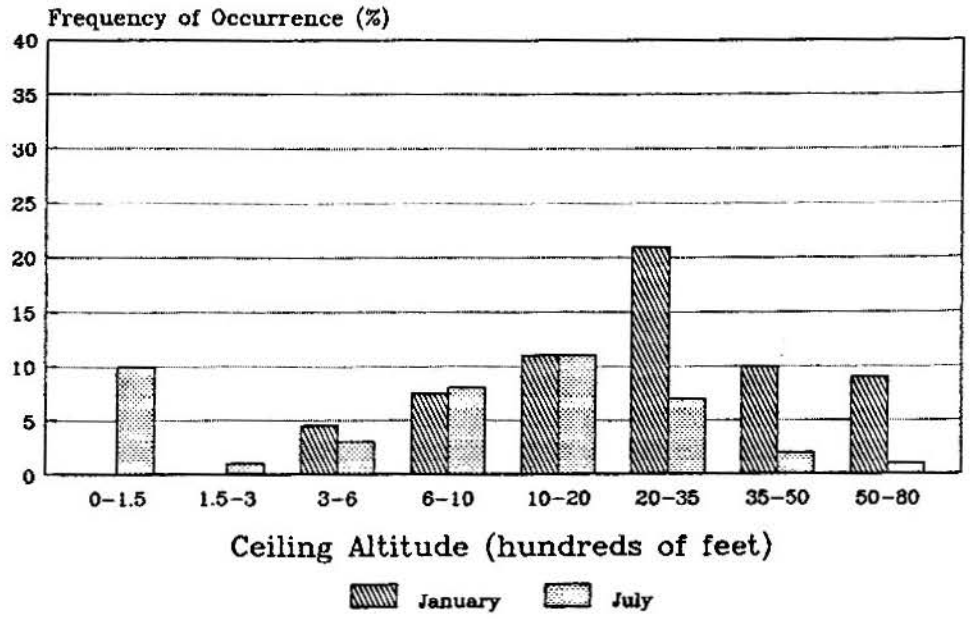

Source: NAVAIR 50-1C-529, Rev 1977

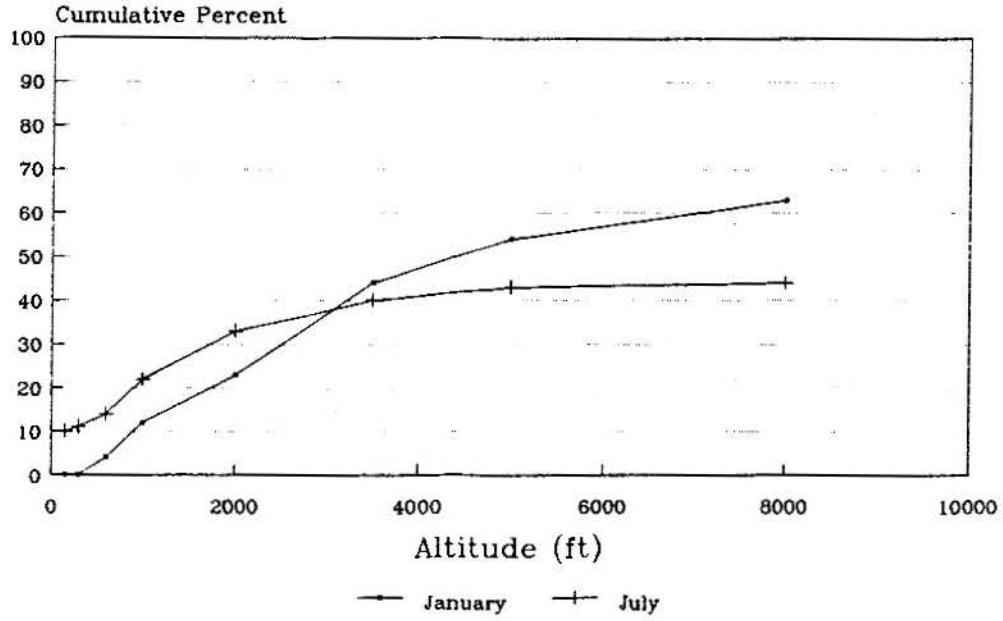

Source: NAVAIR 50-1C-529

Figure 44. Cloud ceiling probabilities over the Yellow Sea (34.9°N, 124.3°E) for the months of January and July

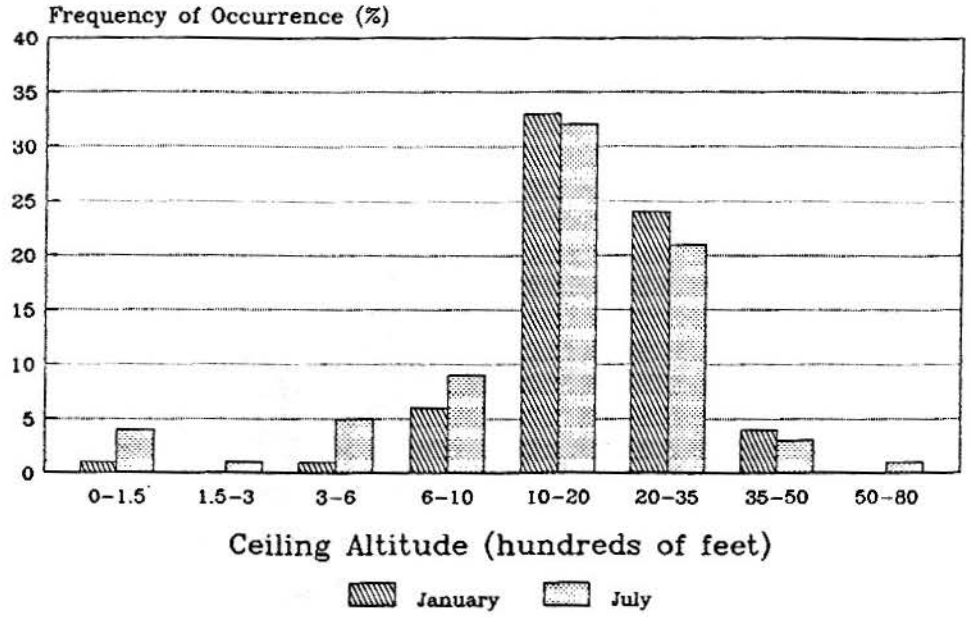

Source: NAVAIR 50-1C-528, Rev 1974

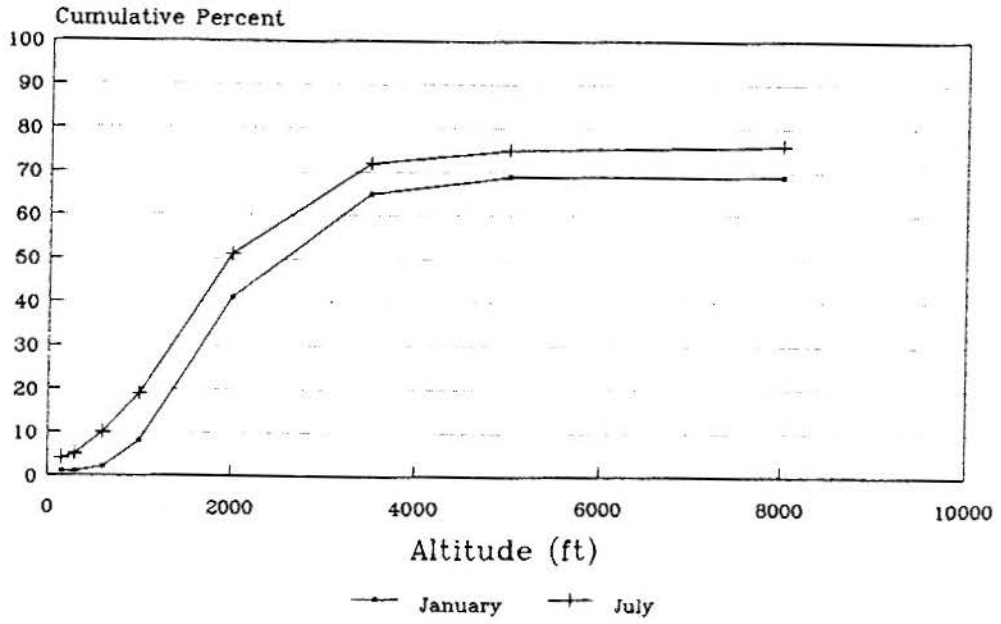

Source: NAVAIR 50-1C-528

Figure 45. Cloud ceiling probabilities over the Norwegian Sea (66.0°N, 2.0°E) for the months of January and July

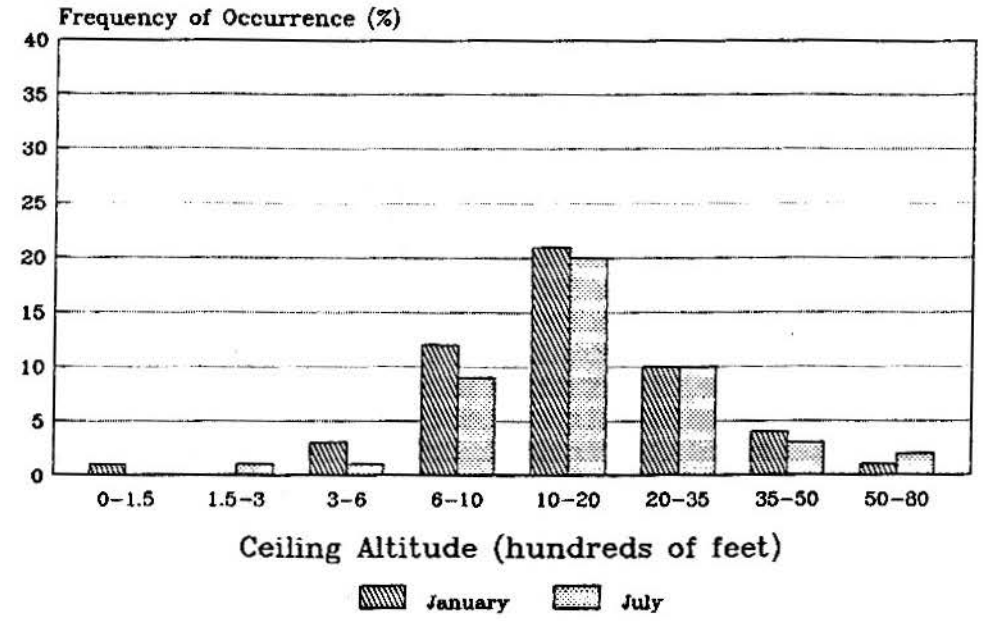

Source: NAVAIR 50-1C-528, Rev 1974

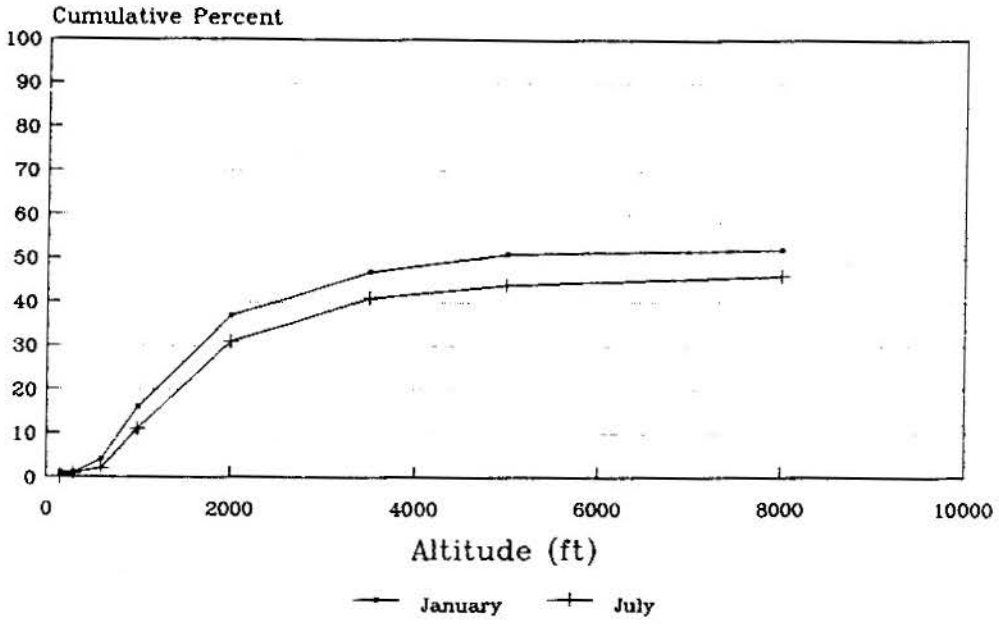

Source: NAVAIR 50-1C-528

Figure 46. Cloud ceiling probabilities east of the Azores (39.0°N, 23.5°W) for the months of January and July

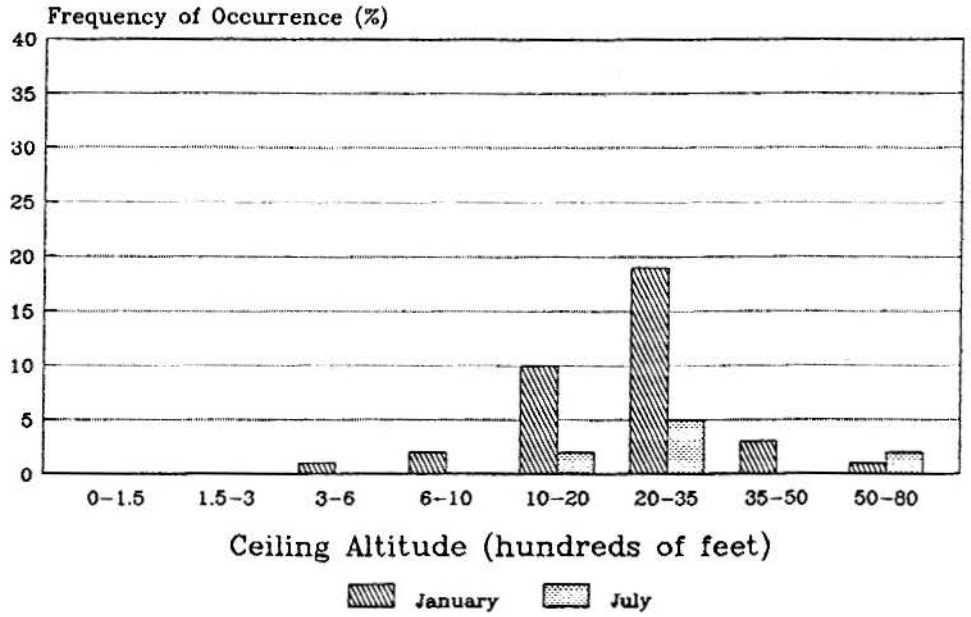

Source: NAVAIR 50-1C-528, Rev 1974

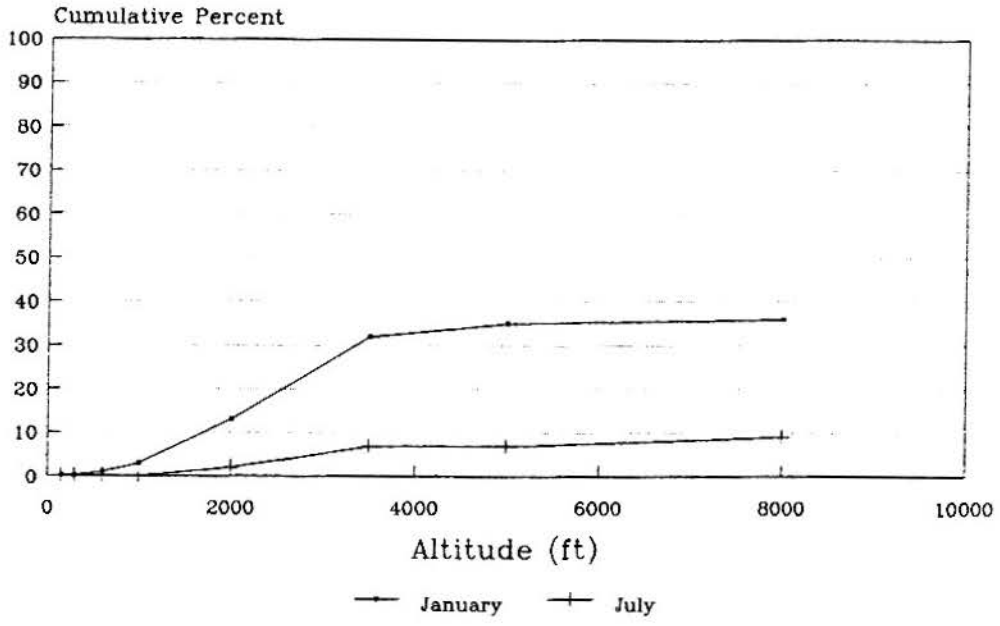

Source: NAVAIR 50-1C-528

Figure 47. Cloud ceiling probabilities over the western Mediterranean Sea (40.0°N, 6.0°E) for the months of January and July

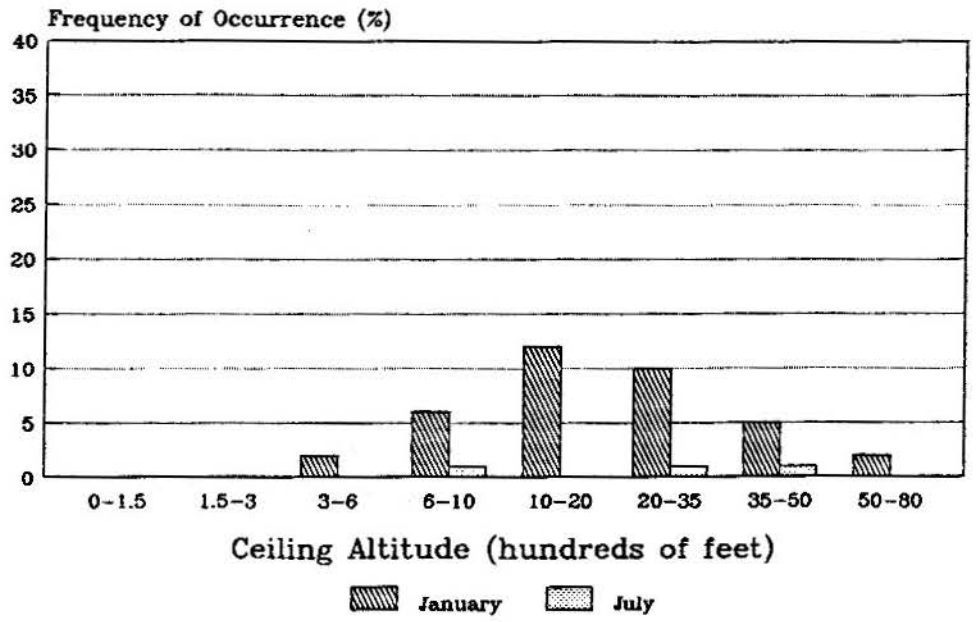

Source: NAVAIR 50-1C-528, Rev 1974

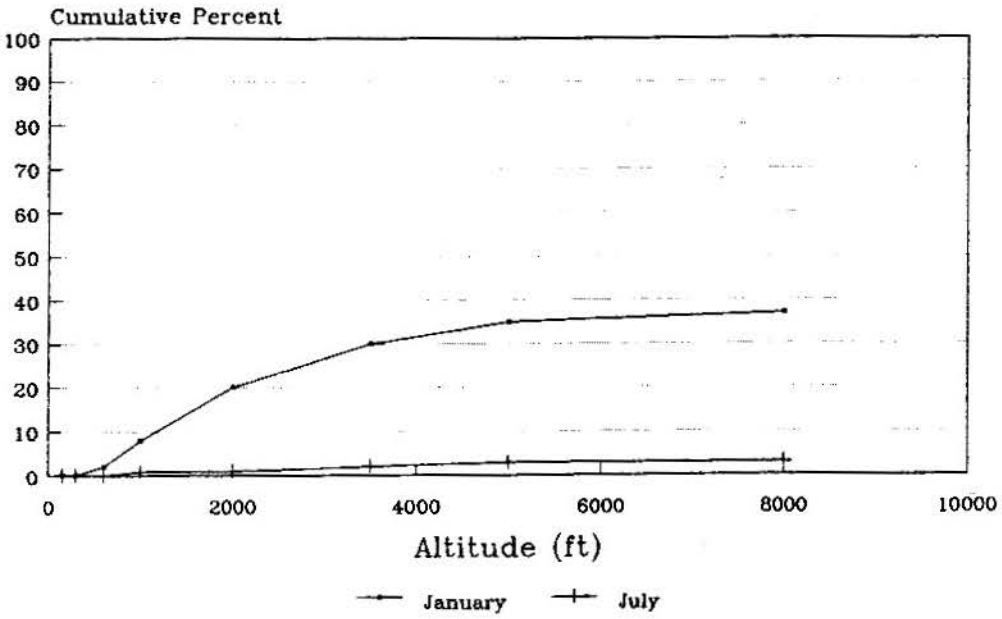

Source: NAVAIR 50-1C-528

Figure 48. Cloud ceiling probabilities over the eastern Mediterranean Sea (35.0°N, 19.0°E) for the months of January and July

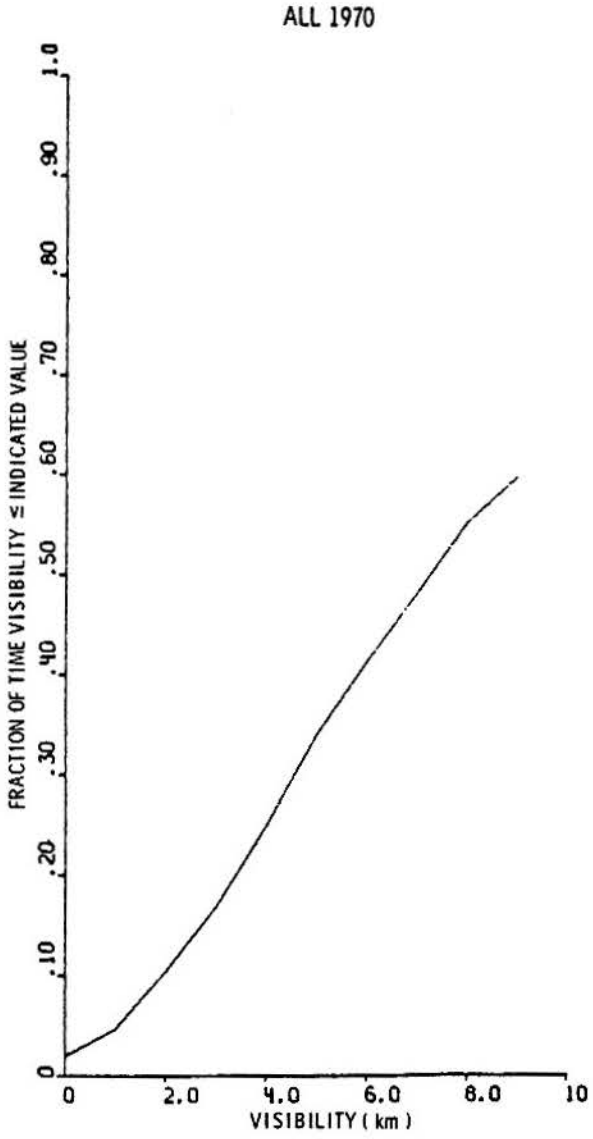

Figure 49. Fractions of the hourly readings for which the visibility at Hannover, Germany, was equal to or less than the indicated distances[10]